JAMES | Journal of Advances in Modeling Earth Systems

RESEARCH ARTICLE
10.1029/2023MS003914

Special Section:
Using radiative-convective equilibrium to understand convective organization, clouds, and tropical climate

Control of Stability and Relative Humidity in the Radiative-Convective Equilibrium Model Intercomparison Project

Allison A. Wing[1] and Martin S. Singh[2]

[1]Department of Earth, Ocean and Atmospheric Science, Florida State University, Tallahassee, FL, USA, [2]School of Earth, Atmosphere and Environment, Monash University, Melbourne, VIC, Australia

Key Points:

- A stability-relative humidity phase space is used to diagnose theory-implied entrainment and precipitation efficiency in RCE
- Variations in entrainment explain intermodel spread in CAPE but variations in precipitation efficiency explain spread in humidity
- Increases in the water vapor scale height with warming lead to CAPE increases with warming that are faster than Clausius-Clapeyron scaling

Supporting Information:

Supporting Information may be found in the online version of this article.

Correspondence to:

A. A. Wing,
awing@fsu.edu

Citation:

Wing, A. A., & Singh, M. S. (2024). Control of stability and relative humidity in the Radiative-Convective Equilibrium Model Intercomparison Project. *Journal of Advances in Modeling Earth Systems*, *16*, e2023MS003914. https://doi.org/10.1029/2023MS003914

Received 2 JUL 2023
Accepted 15 NOV 2023

Abstract The Radiative-Convective Equilibrium Model Intercomparison Project (RCEMIP) exhibits a large spread in the simulated climate across models, including in profiles of buoyancy and relative humidity. Here we use simple theory to understand the control of stability, relative humidity, and their responses to warming. Across the RCEMIP ensemble, temperature profiles are systematically cooler than a moist adiabat, and convective available potential energy (CAPE) increases with warming at a rate greater than that expected from the Clausius-Clapeyron relation. There is higher CAPE (greater instability) in models that are on average moister in the lower-troposphere. To more explicitly evaluate the drivers of the intermodel spread, we use simple theory to estimate values of entrainment and precipitation efficiency (PE) given the simulated values of CAPE and lower-tropospheric relative humidity. We then decompose the intermodel spread in CAPE and relative humidity (and their responses to warming) into contributions from variability in entrainment, PE, the temperature of the convecting top, and the inverse water vapor scale height. Model-to-model variation in entrainment is a dominant source of intermodel spread in CAPE and its changes with warming, while variation in PE is the dominant source of intermodel spread in relative humidity. We also decompose the magnitude of the CAPE increase with warming and find that atmospheric warming itself contributes most strongly to the CAPE increase, but the indirect effect of increases in the water vapor scale height with warming also contribute to increasing CAPE beyond that expected from Clausius-Clapeyron.

Plain Language Summary Idealized model simulations of the tropical atmosphere disagree on profiles of temperature and humidity. Here we use simple theory to understand the intermodel spread in humidity and in a measure of instability to convection (small-scale rising motion). There is greater instability in models that are on average moister. We find that model-to-model variations in small-scale turbulent mixing between cloudy and clear air cause the intermodel spread in instability. Model-to-model variations in the fraction of cloud water that reaches the surface as rainfall cause the intermodel spread in humidity. The instability increases substantially with warming, which is driven by a warmer and moister lower atmosphere.

1. Introduction

The thermodynamic structure of the tropical troposphere has long been known to be strongly influenced by moist convection. Simple models based on a statistical balance between radiative cooling of the atmosphere and heating by convection, known as radiative-convective equilibrium (RCE; Manabe & Strickler, 1964), have been shown to capture important characteristics of the tropical-mean temperature (Singh & O'Gorman, 2013) and humidity (Romps, 2014) profiles. Despite this, uncertainties remain in the response of tropospheric temperature and humidity to warming, and these uncertainties have implications for our understanding of climate model reliability, the response of global-mean surface temperature to an external forcing (climate sensitivity), and changes in severe convective storms with warming.

For example, a persistent discrepancy in the magnitude of enhanced warming in the tropical upper troposphere between satellite observations and historical global climate model simulations (e.g., Douglass et al., 2008; Santer et al., 2008, 2017) has called into question model reliability, among other possible explanations. Enhanced warming of the tropical upper troposphere, associated with a decrease in the rate at which temperature decreases with height (the lapse rate), is expected in a convecting atmosphere where temperature profiles lie near a moist adiabat (Manabe & Stouffer, 1980; Manabe & Wetherald, 1967). This so-called "lapse-rate feedback" acts as a negative feedback on warming since it enables the atmosphere to radiatively cool to space more effectively (Colman & Soden, 2021). At the same time, the water vapor content of the atmosphere increases with warming following the

Clausius-Clapeyron relation, assuming roughly constant relative humidity, and this causes a strong positive feedback on warming (Manabe & Wetherald, 1967). Uncertainty in the combined water vapor-lapse rate feedback is driven largely by model spread in the magnitude and pattern of relative humidity changes in the tropics (Colman & Soden, 2021).

The deviation of the atmospheric thermal stratification from that of an undilute moist adiabat results in convective available potential energy (CAPE), which is an important predictor of severe thunderstorm activity (e.g., Brooks et al., 1994). CAPE is expected to increase in response to warming (Seeley & Romps, 2015; Singh & O'Gorman, 2013), leading to a projected increase in severe thunderstorm activity (Diffenbaugh et al., 2013; Lepore et al., 2021; Singh et al., 2017) and lightning (Romps et al., 2014). But models disagree on the rate at which CAPE increases with warming (Singh et al., 2017), and questions remain as to the ability of climate models to accurately represent CAPE changes, given their difficulties reproducing observed upper-tropospheric temperature trends. For these and other reasons, it is important to improve our understanding of controls on tropical stability and relative humidity and its representation in models.

Here we investigate the stability and humidity distributions in the simple case of RCE as a stepping stone to understanding the full tropical thermodynamic structure. In addition to being the simplest possible way to frame many important questions about the climate system, RCE is valuable by being accessible to a variety of different model types, including those that parameterize convection such as general circulation models (GCMs) and single-column models (SCMs) and those that explicitly simulate convection such as cloud-resolving models (CRMs) and large-eddy simulation (LES) models. This flexibility was recently leveraged to construct the Radiative-Convective Equilibrium Model Intercomparison Project (RCEMIP; Wing et al., 2018; Wing et al., 2020a).

RCEMIP revealed great diversity in the simulated tropical climate, including in mean profiles of temperature, humidity and cloudiness (Wing et al., 2020a). There was no systematic difference between the intermodel spread in models with parameterized convection and those with explicit convection. RCEMIP consisted of a small-domain configuration that generally prohibited convective self-aggregation, which is the spontaneous organization of convection despite homogeneous boundary conditions and forcing (Wing et al., 2017), and a large-domain configuration that permitted self-aggregation. The presence of aggregation has profound effects on the simulated RCE climate, including effects on the radiation balance (Becker & Wing, 2020), precipitation extremes (Pendergrass, 2020), as well as the mean state; the atmosphere is warmer and drier with fewer high clouds when convection is more aggregated (Wing, 2019; Wing et al., 2020a). However, Wing et al. (2020a) reported a large intermodel spread in both tropospheric stability and humidity even among the small-domain RCEMIP simulations that were not aggregated, indicating that processes other than aggregation contribute to variations in the mean state across the ensemble. Here, we focus on the disaggregated case, and we analyze small-domain simulations within the RCEMIP ensemble in order to achieve the following objectives:

1. Document the thermodynamic structure of the mean state across models and under warming in the small domain, unaggregated RCEMIP simulations.
2. Provide a physical understanding of what controls the intermodel spread and what leads to changes in the stability and relative humidity with warming.

In order to address our second objective, we leverage recent theoretical developments that provide a framework within which to interpret differences in the thermodynamic structure of RCE simulations of different models and at different temperatures. Specifically, Singh and O'Gorman (2013) introduced the zero-buoyancy plume model to explain relationships between humidity and lapse rate in RCE (Singh et al., 2019). By including the water budget of the plume and its environment, Romps (2014) developed a full model for the stability and humidity in RCE. According to this model, the thermodynamic structure in RCE is controlled by two main effects: the entrainment and detrainment between moist convection and its environment; and the reevaporation of condensed water produced by convection in the environment. The model therefore allows one to relate differences in stability and humidity in the RCE state to differences in fundamental aspects of moist convection. We will use this framework to investigate the control of stability and relative humidity in the RCEMIP ensemble.

Section 2 briefly reviews the setup of the RCEMIP simulations and examines their thermodynamic structure. Section 3 reviews the relevant theory, introduces a method for diagnosing the theory-implied values of entrainment and precipitation efficiency, and tests this method in a suite of CRM simulations with perturbed physics. Section 4 applies the diagnostic method to the RCEMIP simulations and uses the theory-implied values

Table 1
RCEMIP Simulation Configurations

Simulation type	Model type	Convection	Domain size	Grid spacing	Vertical levels
RCE_small	CRM	Explicit	~100 × ~100 km^2	1 km	~74
RCE_small_vert	VER	Explicit	~100 × ~100 km^2	1 km	~146
RCE_small_les	LES	Explicit	~100 × ~100 km^2	200 m	~146
RCE_small	GCRM	Explicit	52 km radius sphere	1 km	74
RCE_small	SCM	Parameterized	Single Column	N/A	As in CMIP6
RCE_small	WRF-GCM	Parameterized	~100 × ~100 km^2	50 km	48

Note. Each simulation is performed at SST = 295, 300, and 305 K.

of entrainment and precipitation efficiency to attribute the causes of intermodel spread in CAPE and relative humidity. Section 5 decomposes the changes in CAPE with warming into contributions from various factors. Section 6 provides a summary.

2. Thermodynamic Structure in RCEMIP Simulations

2.1. RCEMIP Simulations

Here we briefly review the setup of the RCEMIP simulations. The protocol is fully described by Wing et al. (2018) and an overview of the simulations is provided by Wing et al. (2020a). RCEMIP consists of RCE simulations at three different sea surface temperatures (SST = 295, 300, and 305 K) in two different domains (`RCE_small` and `RCE_large`) across models with explicit convection and those with parameterized convection. The simulations are non-rotating with no land. The SST and insolation are uniform in space and time, and motion is initialized by random noise. Here we consider only the `RCE_small` simulations, whose configurations are summarized in Table 1. By focusing on the `RCE_small` simulations in which convection is quasi-randomly distributed in space and time, we avoid the potentially complicating influence of convective self-aggregation (Wing et al., 2017). We examine 27 sets of simulations with explicit convection and 11 with parameterized convection (see Table S1 in Supporting Information S1 for a list, and the Supporting Information of Wing et al. (2020a) for more detailed descriptions of each model). Of the models examined by Wing et al. (2020a), we exclude several that are missing the data necessary for the analysis here. We also exclude the UKMO-RA1-T simulations at all SSTs and the DALES and DALES-damping simulations at 305 K because these simulations unexpectedly exhibited convective self-aggregation, as evidenced by their broad distribution of precipitable water and column relative humidity variance that is at least an order of magnitude larger than the other `RCE_small` simulations (Wing et al., 2020a). All analysis here is performed using horizontally- and time-averaged fields, with the time average excluding the first 75 days of simulation.

2.2. Thermodynamic Structure

The RCEMIP ensemble exhibits a wide spread in various aspects of the simulated climate, including profiles of temperature and humidity (Figure 1, see also Figures 7 and 8 in Wing et al. (2020a)). This occurs for both models with parameterized convection and those with explicit convection. The temperature profiles are systematically cooler than a moist adiabat, consistent with theory that they are set by dilute ascent, in which entrainment reduces cloud updraft moist static energy (Seeley & Romps, 2015; Singh & O'Gorman, 2013). Here, we compute the moist adiabat by lifting a parcel from the time- and domain-mean temperature and water vapor mixing ratio at the lowest model level assuming no precipitation fallout. We treat ice using a mixed-phase range, in which the fraction of condensate that is frozen increases linearly in temperature between 273.15 and 233.15 K. Since our ice treatment involves a mixed-phase region, the ascent is not reversible, despite all condensate remaining with the parcel. Saturation is calculated assuming air is a Rankine-Kirchoff gas (Romps, 2021), and the lifting condensation level (LCL) pressure is calculated using the method of Romps (2017). The ensemble-mean peak deviation from a moist adiabat in the upper troposphere is between 4 and 10 K, depending on the SST, but this peak deviation varies by ~7–15 K across models (Figures 1a–1c). These deviations from a moist adiabat imply a substantial amount of instability; indeed, the average convective available potential energy (CAPE) at 300 K is 2,022 J kg^{-1}

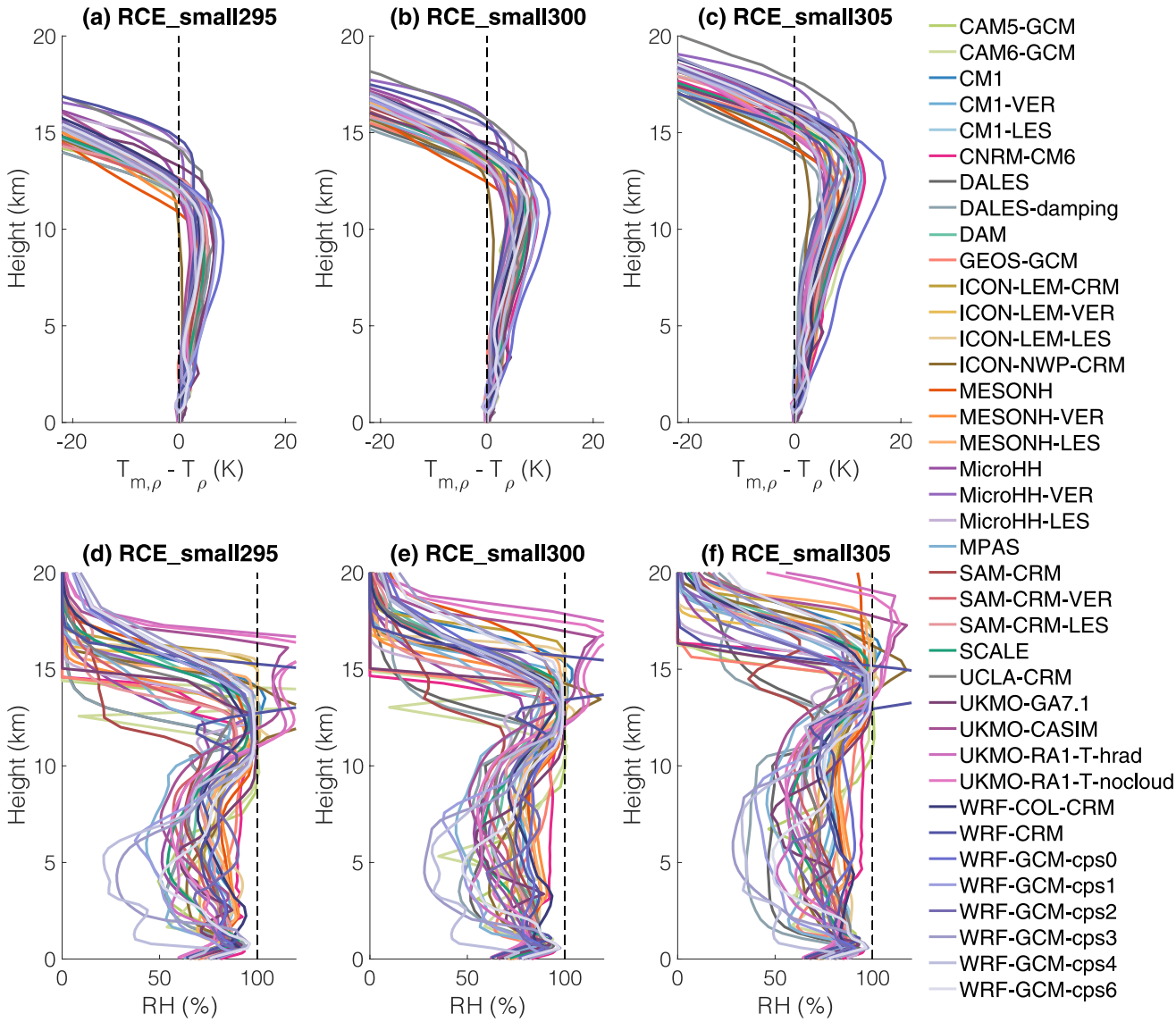

Figure 1. Thermodynamic profiles across the RCEMIP simulations at 295 K (left; a, d), 300 K (center; b, e), and 305 K (right; c, f). Top row (a–c): Difference between the density temperature of a moist adiabat and the time- and domain- mean density temperature in the corresponding simulation. The moist adiabat is computed by lifting a parcel from the lowest model level with no precipitation fallout. Bottom row (d–f): Relative humidity (RH), computed over liquid at temperatures above freezing and over ice at temperatures below freezing, as in Wing et al. (2020a). The *x*-axis is capped at 120% RH.

(Figure 2a). The models with parameterized convection on average have higher CAPE (2,284 J kg^{-1}) than those with explicit convection (1,935 J kg^{-1}), but if one considers the subset of models with explicit convection that have the finest vertical and horizontal grid spacing (the `RCE_small_les` simulations), they have the highest average CAPE values (2,477 J kg^{-1}). This is true also for individual models; each `RCE_small_les` simulation has higher CAPE than its `RCE_small_vert` counterpart, which in turn has higher CAPE than its `RCE_small` counterpart (Figure S5 in Supporting Information S1). As shown in Figure 2a, there is substantial intermodel spread in CAPE; at 300 K the standard deviation across all models is 731 J kg^{-1}.

The relative humidity also varies substantially across models at all SSTs and at all altitudes, including in the lower-troposphere (2–5 km) where at SST = 300 K it ranges from 35% to 90% (Figures 1d–1f). The relative humidity is computed over liquid at temperatures above freezing and over ice at temperatures below freezing, according to each model's formulation for saturation. In the original RCEMIP output, several models inadvertently reported relative humidity with respect to saturation over water at all temperatures. We use the relative humidity values that were corrected by Wing et al. (2020a) to be with respect to saturation over ice at temperatures below

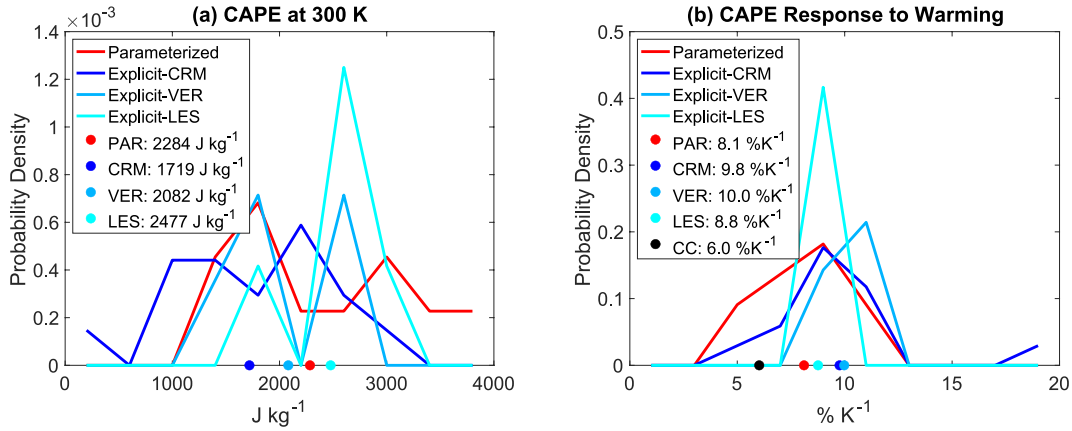

Figure 2. Distribution of CAPE at 300 K (a) and its response to warming (from 295 to 305 K) (b) across the RCEMIP simulations, for models with parameterized convection (PAR; red), models with explicit convection in the `RCE_small` configuration (CRM; dark blue), models with explicit convection in the `RCE_small_vert` configuration (VER; medium blue), and models with explicit convection in the `RCE_small_les` configuration (LES; cyan). The filled circles indicate the mean across each group of models. In panel (b), the black filled circle indicates the Clausius-Clapeyron scaling, based on the percent change in the saturation vapor pressure with warming, evaluated at 300 K.

freezing using the Wagner and Pruß (2002) and Wagner et al. (2011) formulations. Many models are saturated or super-saturated with respect to ice near the tropopause, which is consistent with in situ aircraft-based observations of ice supersaturated regions up to 100 km in scale (Diao et al., 2017). As noted by Wing et al. (2020a), model-to-model variability in near surface relative humidity does *not* explain the spread in the free troposphere (i.e., shifting the profile such that all models start from the same surface value does not reduce the intermodel spread).

As shown in Figures 1a–1c, the buoyancy profiles shift upwards and the average deviation from a moist adiabat increases with warming. This can be seen more clearly in Figures S1–S4 of the Supporting Information S1, which plot the profiles at each SST for individual models. The increase in buoyancy leads to an increase in CAPE with warming, which is on average 9.2% K^{-1} across all models from 295 to 305 K (Figure 2b). We note that there is one outlier with a CAPE scaling of 18.9% K^{-1}; we discuss this further in Section 5. Recent theoretical work has argued that CAPE in RCE increases with warming roughly following the Clausius-Clapeyron rate of increase of saturation vapor pressure, ∼6% K^{-1} (Romps, 2016). While there are some differences in the magnitude of the CAPE increase across models of different types, nearly all models exhibit CAPE increases that are faster than that implied by the Clausius-Clapeyron relation. Romps (2016) pointed out some conditions in which CAPE could increase more quickly with warming, but another possible reason for this discrepancy is that characteristics of convective clouds, such as their mixing and microphysical properties that are assumed constant by Romps (2016), actually change under warming in the simulations. We now seek to quantify how these characteristics vary, both under warming and across the RCEMIP ensemble, by employing a simple model of convection based on an entraining plume.

3. A Model for the Thermodynamic Structure in RCE

We use a model known as the zero-buoyancy plume (ZBP) model, introduced by Singh and O'Gorman (2013) and further developed by Romps (2014), as a diagnostic tool to elucidate how variations in convective entrainment and microphysical processes across the RCEMIP ensemble may explain their mean thermodynamic structure.

3.1. ZBP Theory

The ZBP model describes convection as a steady-state entraining plume in a subsiding environment. It provides a solution for the temperature and humidity structure of the RCE atmosphere by making the twin assumptions that the plume is approximately neutrally buoyant with respect to its environment (Singh & O'Gorman, 2013), and that the humidity of the environment is determined by a balance between moistening through convective detrainment and drying through clear-air subsidence between clouds (Romps, 2014).

According to the ZBP model, the tropospheric lapse rate deviates from a moist adiabat because of the effect of entrainment on air parcels rising through clouds. As the entrainment rate ϵ increases, clouds experience more mixing with the dry environment, and the free troposphere becomes more unstable. The free tropospheric humidity is set by the detrainment of water vapor and cloud water from convection. The environmental humidity therefore depends on the detrainment rate δ and an assumed precipitation efficiency PE, which represents the fraction of condensation that reaches the surface as precipitation, with the remaining cloud water being ejected and evaporating in the environment.

By assuming that the height dependent entrainment rate ϵ_z and the height dependent detrainment rate δ_z are equal, Romps (2016) used the ZBP model to derive an approximate analytic formula for CAPE in RCE that depends on the temperature T_{LCL} and pressure p_{LCL} of the LCL, the temperature of the level of neutral buoyancy T_{LNB}, and the parameter $a = \epsilon_z PE\gamma^{-1}$, where PE is the precipitation efficiency and $\gamma = \partial_z \ln q^*$ is the fractional vertical gradient of saturation specific humidity. To obtain analytic solutions, Romps (2016) took a and PE as constant in the vertical, requiring the vertical variations in ϵ_z to follow those of γ. Here, we diagnose a by considering the values of γ and ϵ_z at the LCL to be inputs, which we denote γ_{LCL} and ϵ, respectively. This implies that ϵ_z increases with height following the decrease of γ^{-1} (the water vapor scale height) with height. While an increase in ϵ_z with height is not entirely realistic (Romps, 2010), estimates of γ from the RCEMIP simulations indicate that most of the increase occurs above 5 km, above the region where the entrainment rate most strongly affects the lapse rate. Thus, while ϵ specifically refers to the entrainment rate calculated at the LCL, we will simply refer to it as the entrainment rate hereafter.

The formula for CAPE is given in full in Equations A1–A4 in Appendix A. A key outcome of the formula is that, for fixed parameters ϵ, PE, γ_{LCL}, and T_{LNB}, CAPE increases with T_{LCL} following Clausius-Clapeyron scaling (Romps, 2016). The ZBP model also provides a formula for the environmental relative humidity that may be written as a simple function of the model parameters as

$$\mathrm{RH} = \frac{\gamma_{\mathrm{LCL}}(1 - \mathrm{PE}) + \epsilon \mathrm{PE}}{\gamma_{\mathrm{LCL}} + \epsilon \mathrm{PE}}. \tag{1}$$

Since we have assumed that a is constant, the relative humidity in our ZBP solutions also does not vary vertically.

The black and gray lines in Figure 3 show the CAPE and relative humidity (RH) predicted by Equations 1 and A1–A4, respectively, for varying entrainment rate ϵ and precipitation efficiency PE and fixed values of γ_{LCL}, T_{LCL}, p_{LCL}, and T_{LNB}. T_{LCL}, p_{LCL}, and T_{LNB} are calculated from model simulations using the methods described above in Section 2.2 to compute the LCL and moist adiabat. γ_{LCL} is determined by computing saturation specific humidity from the simulated temperature and pressure profiles, following the treatment of saturation described above in Section 2.2. The q^* profiles are smoothed using a 5-point running average in the vertical before calculating $\gamma = \partial_z \ln q^*$ using a centered difference in height. The γ profiles are then linearly interpolated to the pressure of the LCL to provide an estimate of γ_{LCL}.

The resultant two-dimensional phase space graphically shows how the instability and environmental humidity of the RCE atmosphere vary with the characteristics of convection. According to the ZBP model, the environmental relative humidity increases with the entrainment rate and decreases with the precipitation efficiency. Since entrainment and detrainment are assumed equal, an increase in entrainment moistens the environment through increased detrainment of water vapor and condensate, while a decrease in precipitation efficiency is associated with greater cloud and rain evaporation in the environment. In contrast, CAPE increases with both the entrainment rate and precipitation efficiency. A higher entrainment rate results in more mixing of the cloud with its environment, leading to a larger lapse rate and CAPE. A higher precipitation efficiency leads to a drier environment, increasing the effect of entrainment on the lapse rate, and also leading to a larger lapse rate. Note that, for fixed precipitation efficiency, CAPE actually increases with the environmental relative humidity. This is because increases in entrainment cause both an increase in CAPE, through their effect on the lapse rate, and an increase in environmental humidity through the increase in convective detrainment.

The CAPE-RH phase space provides a connection between readily diagnosed properties of the RCE simulations and physical parameters of convection such as the entrainment rate and precipitation efficiency. The phase space therefore allows one to investigate the physical mechanisms controlling the variations in stability and humidity both across models and with warming in the RCEMIP ensemble. Before we attempt such an investigation,

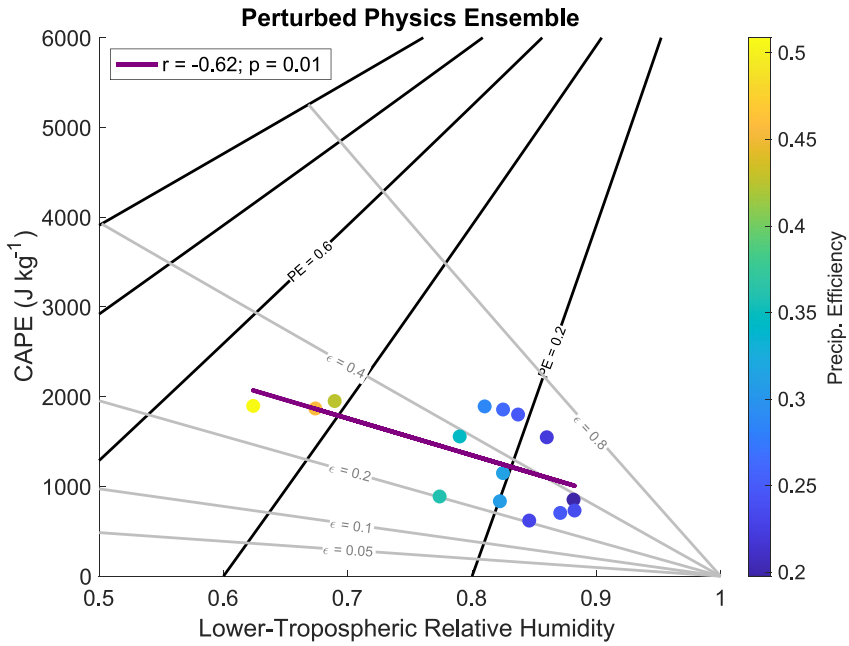

Figure 3. The perturbed physics ensemble in CAPE-RH phase space, based on CAPE and lower-tropospheric relative humidity computed using the domain- and time-mean properties of the simulations. The microphysical precipitation efficiency (PE_{actual}) in these simulations is color shaded. The black and gray lines indicate the values of precipitation efficiency (PE_{theory}) and entrainment (ϵ) implied by ZBP theory, respectively. The purple line indicates a line of best fit, with the linear correlation coefficient indicated in the legend.

however, we demonstrate that the precipitation efficiency derived by applying the ZBP model (theory-implied PE, PE_{theory}) provides a reasonable estimate of the microphysical precipitation efficiency diagnosed directly from precipitation and total condensation (PE_{actual}). A close correspondence between PE_{theory} and PE_{actual} would provide evidence that our theory-based estimates of precipitation efficiency and entrainment rate are capturing real variations of these quantities within the simulations.

3.2. Application to Perturbed Physics Simulations

To test the application of the ZBP theory, we conduct a series of RCE simulations in which we perturb the microphysical parameterization in the model in order to vary the precipitation efficiency. In these simulations, we output the instantaneous microphysical sink of water vapor by condensation in order to calculate the total condensation rate and diagnose the true microphysical precipitation efficiency (PE_{actual}) and compare it to that derived using the ZBP theory (PE_{theory}). Note that RCEMIP did not request the output of gross condensation rates, so we can only diagnose PE_{actual} from this new set of simulations.

A total of 15 simulations are conducted with version 13 of the Cloud Model 1 (CM1; Bryan & Fritsch, 2002) with slight modifications following Singh and O'Gorman (2013) and perturbations to the microphysics scheme described below. This is a different version of the model to that submitted to RCEMIP, but was used because it includes the ability to output microphysical tendencies directly. The simulations are otherwise conducted following the RCEMIP `RCE_small` protocol (Section 2.1; Wing et al., 2018), with a doubly periodic domain of horizontal dimensions 96 km × 96 km, a 1 km horizontal grid spacing, and 74 unevenly spaced vertical levels. Each simulation was run over an SST of 300 K for 100 days, and we present results averaged over the domain and over the last 25 days.

Our control simulation uses a single-moment 5-species microphysics scheme based on that of Lin et al. (1983) as modified by Tao and Simpson (1993) and Braun and Tao (2000), in which the rimed ice species takes the characteristics of hail. We then conduct further simulations in which parameters within the microphysics scheme

Table 2
Parameters Used in Perturbed Physics Simulations

Simulation	A_{mag}	A_{thresh}	V_t (m s^{-1})	PE_{actual}
Control	1	1	–	0.19
1	1	0.01	–	0.22
2	3	0.01	–	0.25
3	5	0.01	–	0.26
4	10	0.01	–	0.29
5	1	1	2	0.23
6	1	1	8	0.25
7	5	1	8	0.43
8	1	1	15	0.24
9	1	0.1	15	0.31
10	1	0.01	15	0.34
11	5	1	15	0.31
12	5	0.01	15	0.46
13	10	1	15	0.36
14	10	0.01	15	0.51

Note. Where the terminal velocity is given as "–," the original terminal velocities calculated by the microphysics scheme are used. The final column gives resultant precipitation efficiency (PE_{actual}).

are perturbed in order to achieve a wide range of precipitation efficiencies in RCE. Specifically, we introduce three parameters that govern the physics perturbations:

1. We multiply the model-calculated autoconversion rates of cloud water to rain and cloud ice to snow by a factor A_{mag}. We further multiply the model's accretion of cloud water by rain drops and accretion of cloud ice by snow by the same factor.
2. We multiply the threshold mass concentration of cloud water below which autoconversion to rain does not occur by a factor A_{thresh}. We further multiply the threshold mass concentration of cloud ice below which snow autoconversion does not occur by the same factor.
3. We set the terminal velocities of all hydrometeors to a value V_t. This change affects the rate at which the hydrometeors fall to the ground, but it does not affect the microphysical process rates, which are calculated using the terminal velocities calculated with the original scheme.

Note that these changes do not directly impact condensation rates within the model, rather they only affect the conversion of condensed water or ice into precipitating hydrometeors. Any dynamical effects on convection are indirect, although they may be substantial nonetheless.

The values of the parameters A_{mag}, A_{thresh}, and V_t for our perturbed physics simulations are given in Table 2. Note that the range of values we simulate is not intended to represent plausible values of microphysical parameters but is simply used to ensure the resultant precipitation efficiency varies over as wide a range as possible. We define PE_{actual} as the domain- and time-mean precipitation rate divided by the domain- and time-mean gross condensation rate. We evaluate this directly using outputs of the microphysical sink of water vapor for each simulation (Table 2), giving values in the range 0.19 in the control to 0.51 in the simulation with the highest PE_{actual}.

The results of our perturbed physics simulations are plotted on the CAPE-RH phase space in Figure 3. Here the theoretical curves (black and gray lines) are calculated based on the mean values of γ_{LCL}, T_{LCL}, p_{LCL}, and T_{LNB} across the perturbed-physics ensemble. The simulated value of RH is taken as a mass-weighted mean between 2 and 5 km, since we expect the lower-tropospheric humidity to be most influential in determining the lapse rate throughout the troposphere (Seeley & Romps, 2015). We explored the sensitivity to averaging RH over various ranges of heights between 1 and 6 km, and while the actual values vary, our conclusions below are robust to the choice of heights. The CAPE is calculated as the integral of the positive buoyancy from a parcel initialized from the lowest model level and lifted adiabatically without precipitation fallout to the level of neutral buoyancy as described in Section 2.

Both RH and CAPE vary across the perturbed physics simulations, with higher PE_{actual} (represented by colors) generally corresponding to lower RH and higher CAPE. The simulations lie roughly along the $\epsilon = 0.3$ km^{-1} line, which is a good match to direct measurements of entrainment in modeling studies (e.g., Romps, 2010). This suggests that the bulk of the variations in CAPE and RH in the simulations are driven by variations in precipitation efficiency. This is consistent with the nature of the perturbations, which directly affect only the conversion of cloud condensate to precipitation, and not the dynamics, and it provides support for the ZBP model as giving reasonable diagnoses of precipitation efficiency across the simulations. However, we note that the theory-implied entrainment is also affected by our microphysical perturbations, varying by more than a factor of two across the simulations.

To calculate PE_{theory} in a more quantitative way, we plot each perturbed physics simulation within a CAPE-RH phase space calculated using the values of γ_{LCL}, T_{LCL}, p_{LCL}, and T_{LNB} taken from the corresponding simulation (not shown). We then estimate the ϵ and PE contours that pass through the location of the simulation in phase space to derive a theory-implied value of the entrainment rate and precipitation efficiency (PE_{theory}).

Figure 4a shows that PE_{theory} is closely related to PE_{actual}, with a correlation coefficient of 0.96 across the perturbed physics ensemble. Moreover, the results lie relatively close to the one-to-one line, indicating PE_{theory} is a good

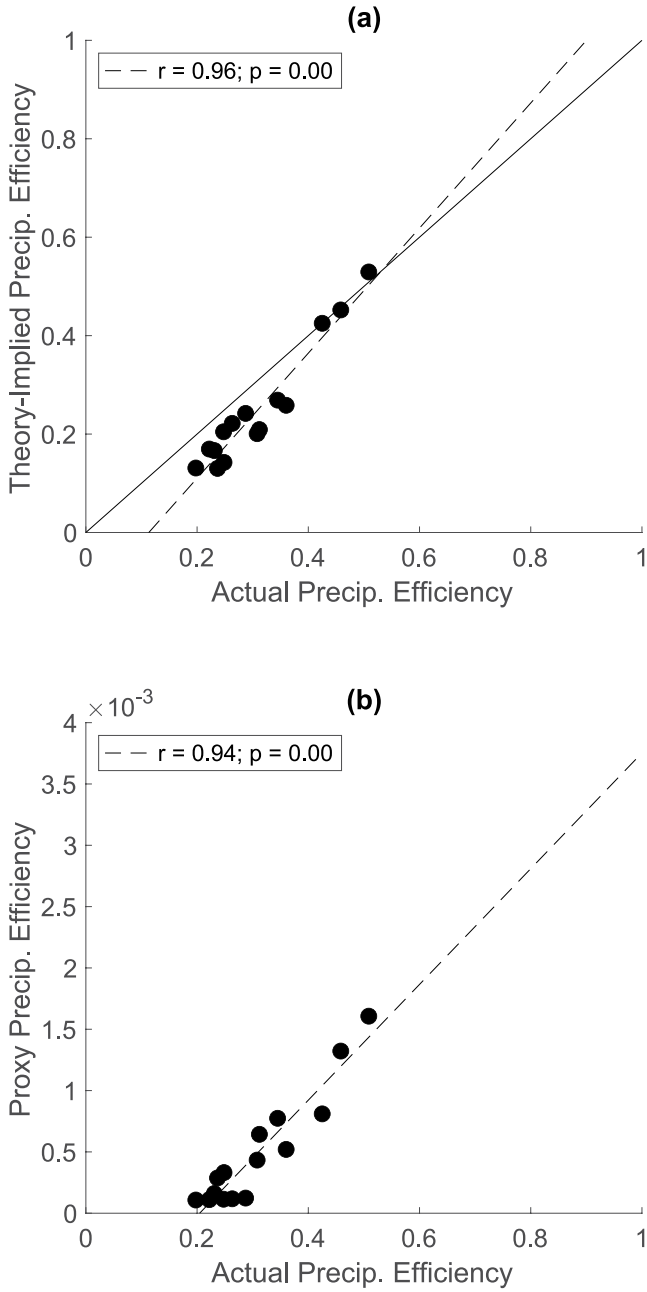

Figure 4. Relationship between PE_{actual} in the perturbed physics ensemble and (a) the precipitation efficiency implied by ZBP theory (PE_{theory}) and (b) the precipitation efficiency proxy (PE_{proxy}; s^{-1}).

estimate of PE_{actual}, although PE_{actual} is slightly underestimated, particularly when it is low. Nevertheless, the close correspondence of PE_{theory} to PE_{actual} strengthens our confidence in using the CAPE-RH phase space to derive physical parameters of moist convection within the RCE simulations. In Section 4, we will apply this method to the RCEMIP ensemble, and we will use it to diagnose the physical mechanisms affecting humidity and stability across the ensemble.

Finally, we derive a proxy for the precipitation efficiency (PE_{proxy}) that is independent of the ZBP model but can be calculated from standard model outputs and can thus be applied to the RCEMIP simulations. The definition of the microphysical precipitation efficiency (PE_{actual}) may be written

$$\mathrm{PE}_{\mathrm{actual}} = \frac{P}{P+E}, \tag{2}$$

where P is the domain-averaged surface precipitation rate and E is the domain-mean, column-integrated rate of evaporation of cloud and precipitation condensates. We now make a simple parameterization for E as an exponential decay of the total column condensed water W. That is,

$$E = \frac{W}{\tau} \tag{3}$$

for some evaporation timescale τ. We therefore may write the precipitation efficiency

$$\mathrm{PE}_{\mathrm{actual}} \approx \frac{\frac{\tau P}{W}}{1+\frac{\tau P}{W}}. \tag{4}$$

Approximating the timescale τ as a constant and assuming that PE_{actual} is small, as is generally true in the simulations, the precipitation efficiency will roughly scale as

$$\mathrm{PE}_{\mathrm{actual}} \propto \frac{P}{W}. \tag{5}$$

We therefore define a proxy for the precipitation efficiency as $PE_{proxy} = P/W$. This is identical to the macro-scale precipitation efficiency defined by Li et al. (2022), except that here we include precipitating condensates in the definition of W in addition to cloud condensate. Note that PE_{proxy} has units of s^{-1}, and we therefore cannot compare its absolute value to PE_{actual} (which is unitless).

For the perturbed physics ensemble, there is a strong relationship between PE_{actual} and PE_{proxy}, with a correlation of 0.94 across the ensemble. We therefore will use PE_{proxy} as an alternative estimate of the precipitation efficiency that can be estimated for the RCEMIP ensemble and used to compare to PE_{theory} derived from the ZBP model.

As an aside, we note that, across simulations with the model used for the perturbed physics ensemble (CM1) at different SSTs, PE_{theory} and its correspondence with PE_{actual} and PE_{proxy} is sensitive to which heights are used to diagnose the lower-tropospheric RH (not shown). This is because in CM1, the change in RH with warming switches sign around 4.5 km. PE_{actual} and PE_{proxy} increase modestly with warming in CM1, but this is only captured by PE_{theory} if RH is averaged below 4.5 km. This is consistent with the notion that the precipitation efficiency PE_{actual} is most sensitive to microphysical processes in the lower troposphere, where the bulk of the condensation occurs. We emphasize though that the correspondence between PE_{actual}, PE_{theory}, and PE_{proxy} across the perturbed physics ensemble at a given SST, which is *not* sensitive to the precise heights used, is strong evidence for the

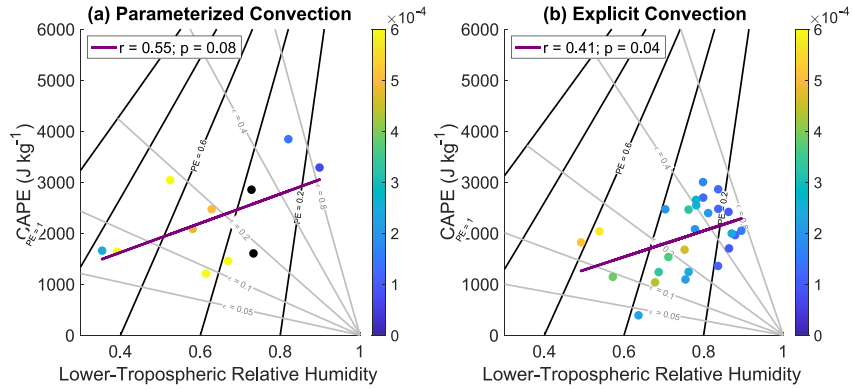

Figure 5. The RCEMIP ensemble in CAPE-RH phase space based on CAPE and lower-tropospheric relative humidity, for (a) models with parameterized convection and (b) models with explicit convection. The proxy precipitation efficiency (PE_{proxy}; s^{-1}) is color shaded; models without the data necessary to compute the proxy precipitation efficiency are shown in black. The black and gray lines indicate the values of precipitation efficiency (PE_{theory}) and entrainment (ϵ) implied by ZBP theory, respectively. The purple line indicates a line of best fit, with the linear correlation coefficient indicated in the caption.

validity of using the ZBP theory to diagnose PE_{theory}. Further, we also tested the results presented below in Sections 4 and 5 to the heights over which RH is averaged, considering 42 different height ranges in which the lower bound is drawn from [1 km: 0.5 km: 4 km] and the upper bound is drawn from [3 km: 0.5 km: 6 km]. None of the broad conclusions are qualitatively sensitive to the heights used (not shown), indicating that it is perhaps just bad luck that the dependence of RH and thus PE_{theory} with warming in CM1 is strongly sensitive to height.

4. Contributions to Intermodel Spread in Thermodynamic Structure

We now apply the methodology described and tested in Section 3 to diagnose the theory-implied values of entrainment and precipitation efficiency (PE_{theory}) in the RCEMIP simulations and decompose the intermodel spread in CAPE, relative humidity, and their changes with warming into contributions from model-to-model variability in various factors.

4.1. CAPE-RH Phase Space

First we construct the CAPE-RH phase space for the RCEMIP simulations, and use this to diagnose the theory-implied values of entrainment and precipitation efficiency (PE_{theory}), as shown in Figure 5. As in Figure 3, the ϵ and PE_{theory} lines in Figure 5 are computed using the model-mean values of γ_{LCL}, T_{LCL}, p_{LCL}, and T_{LNB}, as a representative visual. However, when we diagnose the values of entrainment and PE_{theory} for each model, we compute the theoretical CAPE and relative humidity from the model-specific values of the LCL and LNB (effectively we create a separate version of Figure 5 for each model). This is more accurate, though the results are qualitatively similar if the model-mean values are used instead. The lower-tropospheric relative humidity and CAPE are computed in the same manner as for the perturbed physics simulations described in Section 3.2.

Figure 5 demonstrates that models with higher lower-tropospheric relative humidity have higher values of CAPE (i.e., more instability). The correlation is statistically significant at the 95% level for models with explicit convection and at the 90% level for models with parameterized convection. This relationship is counterintuitive, as one might have expected that, in a moister atmosphere, entrainment would be less effective at reducing cloud updraft moist static energy, allowing the atmosphere to convect closer to a moist adiabat and thus have lower CAPE. This would be the case if relative humidity were imposed externally (as in Singh and O'Gorman (2013) and Seeley and Romps (2015)) or if the value of entrainment was fixed (i.e., along a gray line in Figure 5). However, when CAPE and relative humidity are both determined internally, they are *both* influenced by *both* entrainment and PE (Section 3). And, as is clear from Figure 5, neither entrainment nor PE_{theory} appear fixed across models (the scatter points fall on neither the black nor gray lines). As discussed in Section 3, if PE_{theory} were fixed (following the black lines in Figure 5), then the theory predicts that higher entrainment would lead to both higher CAPE and higher relative humidity. This is the same sign as the relationship found in the RCEMIP simulations, suggesting

that the CAPE-RH relationship is driven by different values of entrainment across models. However, the slope of the line of best fit for RCEMIP is less steep than the PE_{theory} contours, indicating that variations in PE_{theory} across models also contribute.

The color shading in Figure 5 shows PE_{proxy} (Section 3.2). While the values are not directly comparable, the PE_{proxy} values tend to increase from right to left in CAPE-RH phase space, approximately following increasing PE_{theory}. The correlation between PE_{theory} and PE_{proxy} is $r = 0.81$ for models with explicit convection (not shown), which, while statistically significant at the 99% level, is not quite as strong as that for the perturbed physics simulations (Figure 4b). The correlation for models with parameterized convection is $r = 0.58$ (statistically significant at the 90% level), but this correlation is entirely driven by two outlier models. The weaker relationship between PE_{theory} and PE_{proxy} in RCEMIP could reflect shortcomings in PE_{proxy} when applied to the diverse spectrum of RCEMIP models or inaccuracies in the ZBP theory (Section 3). While we were careful to compute PE_{proxy} with the correct condensed water outputs from each model, we also cannot rule out errors in the RCEMIP output. There is a large spread in PE_{proxy} values across the RCEMIP simulations, particularly for the models with parameterized convection (the colorbar is saturated at 6×10^{-4} s^{-1}; the largest value is 9×10^{-3} s^{-1}). The relationship between PE_{theory} and PE_{proxy} across the RCEMIP ensemble is robust to the range of heights used to estimate the lower-tropospheric RH (not shown). Further, Figures S1–S4 in Supporting Information S1 show that the ZBP model has skill in reproducing the vertical structure of parcel buoyancy within each model. In particular, the ZBP model reproduces the increase and deepening of the buoyancy profiles with warming as seen in the simulations, and has some skill in matching the buoyancy magnitudes simulated by each model. The agreement is a bit better if, rather than assuming the vertical variation in ϵ_z matches that of γ, we instead assume constant entrainment with height, but this would preclude the analytical CAPE decomposition in Section 5. These results provide further support for our use of the ZBP model to diagnose entrainment and precipitation efficiency from the simulations.

We also note that the relationship between CAPE and relative humidity is qualitatively similar if just the subset of models with `RCE_small_vert` and `RCE_small_les` versions is used (Figure S5 in Supporting Information S1), though the correlations are no longer significant given the small sample size. There are not any notable dependencies of relative humidity or theory-implied entrainment and PE_{theory} on the vertical and horizontal resolution, but there is a tendency for CAPE to increase with finer vertical and horizontal grid spacing, as also noted above in Section 2.

4.2. Intermodel Spread of CAPE and RH

In order to more quantitatively attribute the intermodel spread in CAPE and RH to model-to-model variations in entrainment or PE_{theory}, we use the ZBP model (Equations 1 and A1–A4) to recompute the theoretical CAPE and relative humidity values in which we allow only one of the parameters (ϵ, PE_{theory}, T_{LNB}, γ_{LCL}) to vary across models. For instance, to assess the role of entrainment in explaining the intermodel spread, we calculate the theoretical CAPE and relative humidity for each model using the model-specific values of theory-implied entrainment that we diagnosed, but the model-mean values of PE_{theory}, γ_{LCL}, and T_{LNB}.

If one uses the model-specific values of all parameters to compute the theoretical CAPE this returns the simulated CAPE since the ZBP model is, by construction, able to reproduce the CAPE and RH values from the simulations given the diagnosed parameters ϵ and PE_{theory}. By comparing the correlation coefficients and range of theoretical CAPE values in Figure 6, in which *only* γ_{LCL}, or only T_{LNB}, or only PE_{theory}, or only the entrainment are allowed to vary, we can determine which parameter exerts the strongest control on the intermodel spread in CAPE. If a parameter returns a theoretical CAPE with a wide range of values, this indicates that model-to-model variations in that parameter have a strong effect on CAPE. However, to drive the actual model-to-model variation in CAPE, there must also be a strong correlation between that version of theoretical CAPE and the simulated CAPE.

The highest correlation and widest range of theoretical CAPE values is found in Figure 6d, indicating that model-to-model variations in entrainment are the most important factor controlling the intermodel spread in CAPE. Significant correlations are also found in Figures 6a and 6b (moreso for the CRMs than the models with parameterized convection), indicating that model-to-model variation in γ_{LCL} and T_{LNB} (related to the temperature depth of the troposphere) also contributes to the intermodel spread in CAPE, though over a smaller range of values. The theoretical CAPE calculated with varying PE_{theory} exhibits a wide range of values, but it is uncorrelated with the simulated CAPE. This indicates that variations in PE_{theory} have a strong effect on CAPE, but do not drive the overall trend across models.

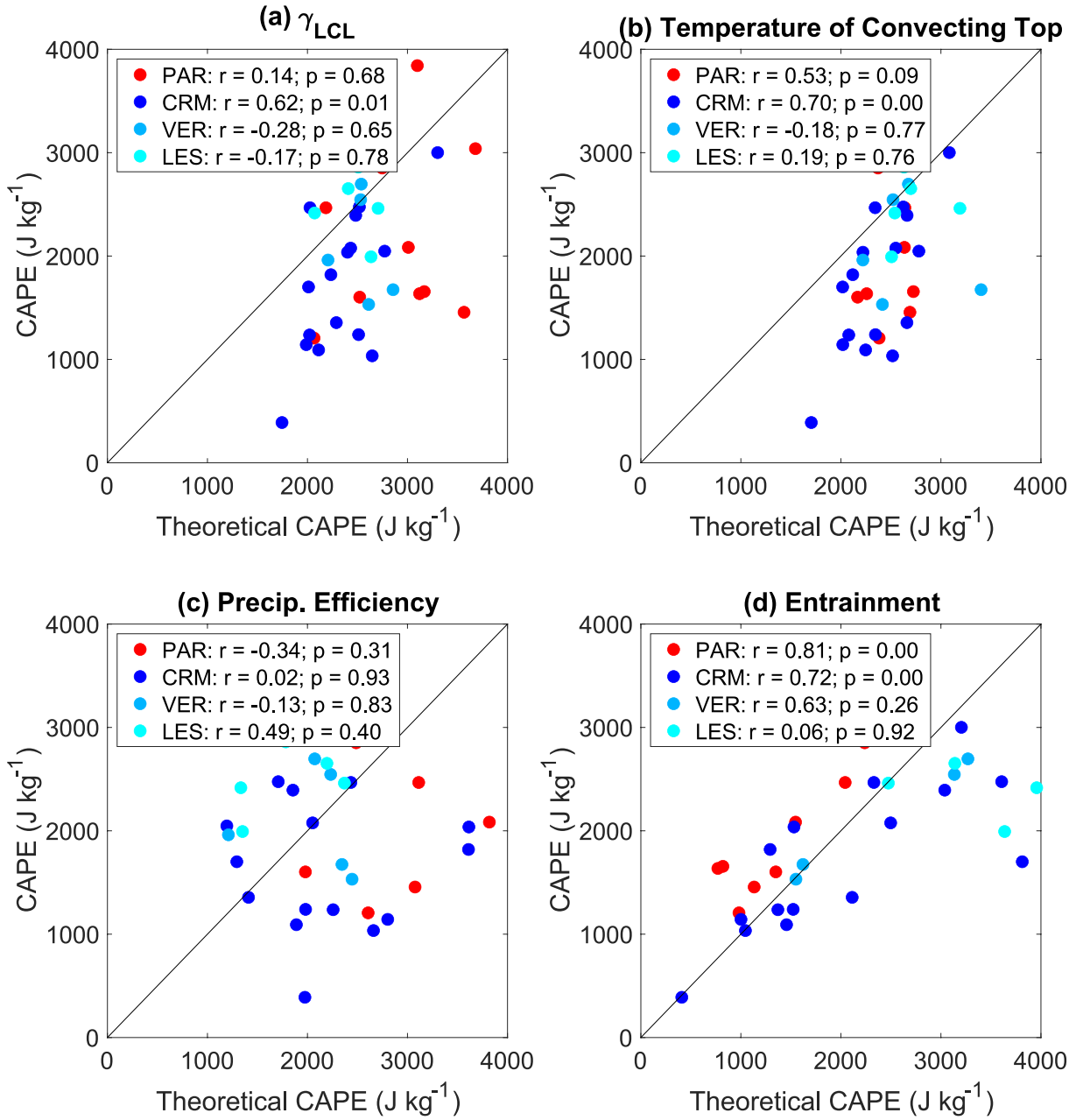

Figure 6. Decomposition of intermodel spread in CAPE at 300 K into contributions from intermodel variability in (a) γ_{LCL}, (b) temperature of the convecting top, (c) precipitation efficiency (PE_{theory}), and (d) entrainment, for models with parameterized convection (PAR; red), models with explicit convection in the `RCE_small` configuration (CRM; dark blue), models with explicit convection in the `RCE_small_vert` configuration (VER; medium blue), and models with explicit convection in the `RCE_small_les` configuration (LES; cyan).

Figures 7a and 7b performs the same exercise for relative humidity. We exclude the contribution from intermodel variability in T_{LNB} since the equation for relative humidity (Equation 1) does not include this parameter. We also do not show the contribution from intermodel variability in γ_{LCL} because it is small. When allowing either PE_{theory} or entrainment to individually vary, both versions of the theoretical relative humidity have strong, statistically significant correlations with the simulated relative humidity (Figures 7a and 7b). However, variations in entrainment result in only a small range of theoretical relative humidity values, whereas the contribution from PE_{theory} variations results in a wider range of theoretical relative humidity values that lie close to the 1:1 line and exhibit a higher correlation with simulated relative humidity ($r = 0.98$ for models with parameterized convection and $r = 0.99$ for models with explicit convection). That is, we can nearly recover the relationship between simulated

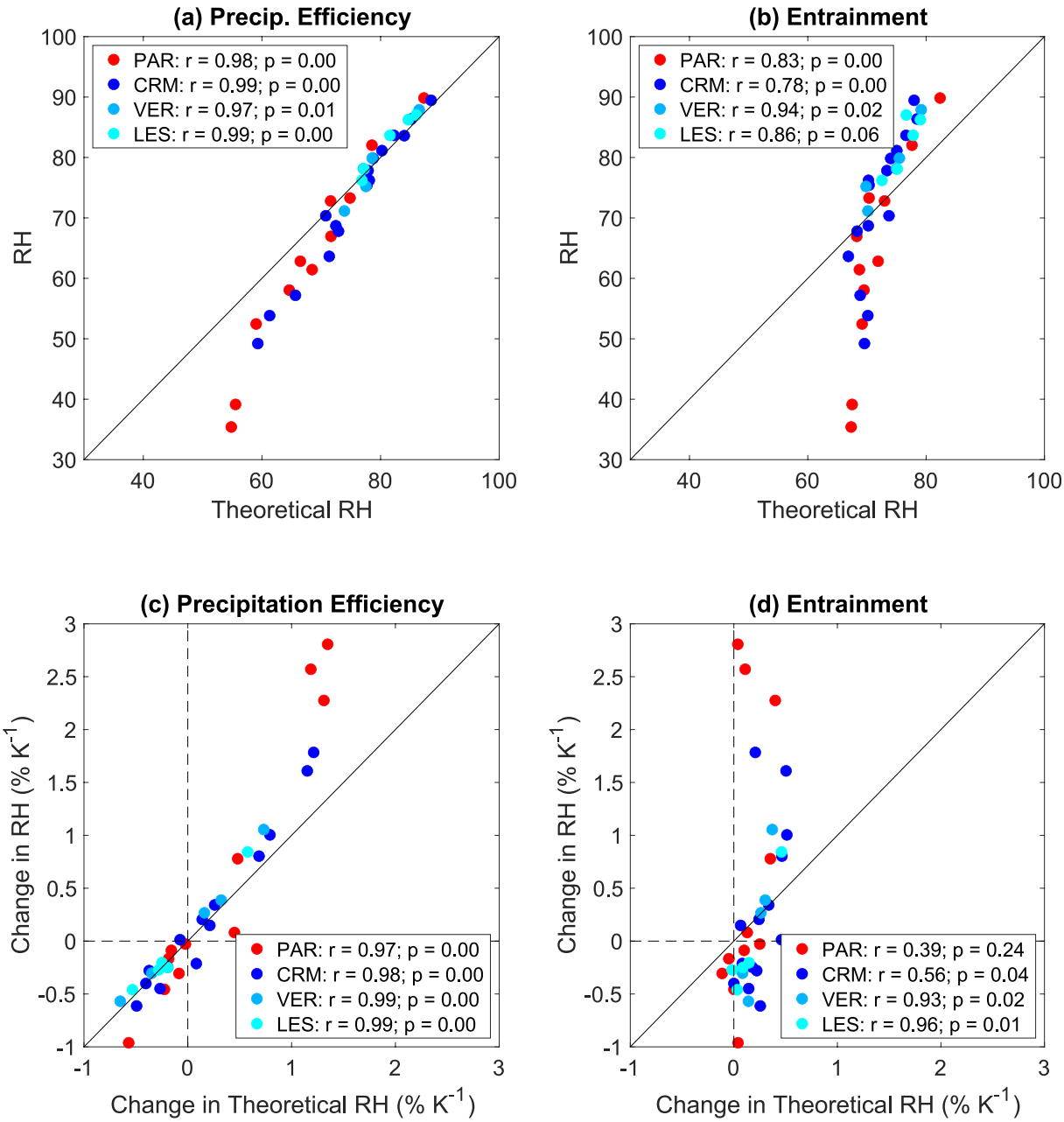

Figure 7. Decomposition of intermodel spread in relative humidity at 300 K (top row; a, b) and its changes with warming (bottom row; c, d) into contributions from intermodel variability in (left column; a, c) precipitation efficiency (PE_{theory}), and (right column; b, d) entrainment, for models with parameterized convection (PAR; red), models with explicit convection in the `RCE_small` configuration (CRM; dark blue), models with explicit convection in the `RCE_small_vert` configuration (VER; medium blue), and models with explicit convection in the `RCE_small_les` configuration (LES; cyan).

and theoretical relative humidity by considering *only* model-to-model variations in PE_{theory}. Therefore, while model-to-model variation in entrainment does contribute, model-to-model variation in PE_{theory} is the dominant factor controlling intermodel spread in relative humidity.

4.3. Intermodel Spread of Changes in CAPE and RH With Warming

Next, we consider the intermodel spread in the *changes* in CAPE with warming. This is assessed by comparing the change in simulated CAPE with the change in the various versions of theoretical CAPE between 295 and 305 K. For example, to diagnose the role of model-to-model variability in entrainment, we compute theoretical

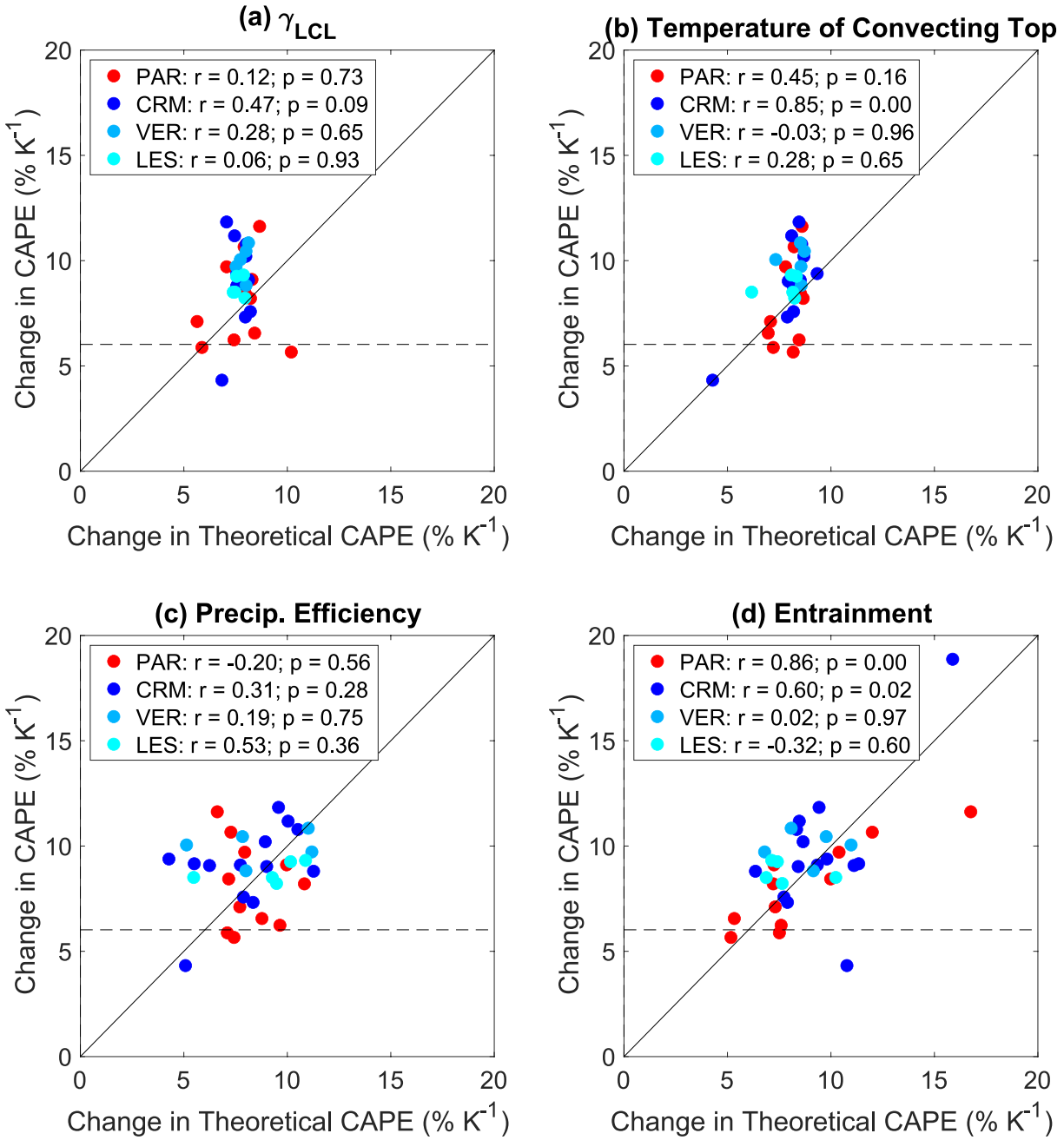

Figure 8. Decomposition of intermodel spread in changes in CAPE with warming into contributions from intermodel variability in changes in (a) γ_{LCL}, (b) temperature of the convecting top, (c) precipitation efficiency (PE_{theory}), and (d) entrainment, for models with parameterized convection (PAR; red), models with explicit convection in the `RCE_small` configuration (CRM; dark blue), models with explicit convection in the `RCE_small_vert` configuration (VER; medium blue), and models with explicit convection in the `RCE_small_les` configuration (LES; cyan).

CAPE at 305 and 295 K using the model-specific entrainment values and model-mean γ_{LCL}, PE_{theory}, and T_{LNB} at each of those temperatures, and we then take the difference between the two. This isolates the effects of model-to-model variability in entrainment, but it still allows all parameters to change with warming.

All of the models exhibit increases in CAPE with warming, but the rates vary between 4.3% and 11.8% K^{-1}, with an outlier at 18.9% K^{-1} (Figures 2 and 8). For models with parameterized convection, the only significant correlation occurs when entrainment is allowed vary across models (Figure 8d). Further, the outlier only emerges when entrainment is allowed to vary across models; see Section 5 for more discussion. However, for models with

explicit convection, the change in theoretical CAPE with warming captures some of the variability in the change in simulated CAPE with warming both when T_{LNB} varies across models and when entrainment does (Figures 8b and 8d), and, to a lesser extent, γ_{LCL} (Figure 8a). The correlation is actually stronger for T_{LNB} ($r = 0.85$) than entrainment ($r = 0.60$), which seemingly implies that model-to-model variability in T_{LNB} at different SSTs contributes most to the intermodel spread in the CAPE changes. However, when T_{LNB} varies across models, the range of values of the change in theoretical CAPE is small. Model-to-model variations in PE_{theory} do influence the range of values of the change in theoretical CAPE, but these are uncorrelated with the simulated CAPE (Figure 8c). Thus, as was the case for CAPE itself, we conclude that model-to-model variability in entrainment at different SSTs contributes most to the intermodel spread in the CAPE changes with warming.

Finally Figures 7c and 7d decomposes the intermodel spread in the changes in relative humidity with warming. Lower-tropospheric relative humidity changes only slightly with warming; the average rate across all models is 0.3% K^{-1}, with a 5%–95% confidence interval of 0.03%–0.6% K^{-1} and range from −0.9% to 2.8% K^{-1} (see y-axis in Figures 7c and 7d). All the models with relative humidity increases greater than 2% K^{-1} are models with parameterized convection. As was the case for the intermodel spread in relative humidity itself, model-to-model variations in PE_{theory} dominate the intermodel spread in changes in relative humidity.

As an aside, we note that changes in PE_{theory} with warming are uncorrelated with changes in PE_{proxy} with warming (not shown). PE_{proxy} increases with warming across most of the models, consistent with Li et al. (2023), but PE_{theory} instead decreases in about half the models (changes in PE_{theory} range from −4.0% to 3.2% K^{-1}). The large changes in PE_{proxy} with warming (half the models have increases greater than 4% K^{-1}) would imply larger changes in relative humidity than are found (Figures 7c and 7d). Thus, if one assumes that the theory for relative humidity is accurate, this would seem to cast some doubt on the ability of PE_{proxy} to capture changes with climate warming. However, the change in PE_{theory} with warming is slightly sensitive to the range of heights used to derive the lower-tropospheric average RH; if lower heights are used (below 3 km), then there is a weak positive correlation between PE_{theory} and PE_{proxy}. Therefore, we cannot rule out the possibility of increases in precipitation efficiency with warming.

5. Decomposition of CAPE Response to Warming

Section 4.3 applied a decomposition to explain the intermodel spread in the changes in CAPE and relative humidity with warming. Here, we instead consider the *magnitude* of the CAPE response to warming and seek to explain why it increases and why, on average and in nearly all individual models, it does so at a rate greater than that expected from the Clausius-Clapeyron relation (Figures 2 and 8).

We decompose the response of CAPE to warming $\left(\frac{d\text{CAPE}}{dT}\right)$ by considering the dependence of CAPE on the six parameters in the framework of the ZBP theory: T_{LCL}, p_{LCL}, T_{LNB}, ϵ, PE and γ_{LCL}) (Section 3, Romps, 2016). Thus, the response of CAPE to warming is given by:

$$\frac{d\text{CAPE}}{dT} = \frac{dT_{LCL}}{dT}\frac{\partial\text{CAPE}}{\partial T_{LCL}} + \frac{dp_{LCL}}{dT}\frac{\partial\text{CAPE}}{\partial p_{LCL}} + \frac{dT_{LNB}}{dT}\frac{\partial\text{CAPE}}{\partial T_{LNB}} + \frac{d\epsilon}{dT}\frac{\partial\text{CAPE}}{\partial\epsilon} + \frac{d\text{PE}}{dT}\frac{\partial\text{CAPE}}{\partial\text{PE}} + \frac{d\gamma_{LCL}}{dT}\frac{\partial\text{CAPE}}{\partial\gamma_{LCL}}. \quad (6)$$

The partial derivatives in Equation 6 are derived analytically from Equations A1–A4 (see Appendix A) and evaluated based on the values of the parameters at 300 K. The response to warming of each of the parameters and CAPE itself (the total derivatives in Equation 6) are evaluated based on the difference in the simulated values and theory-implied values for ϵ and PE (PE_{theory}) between the 295 and 305 K simulations. The response of CAPE to warming $\left(\frac{d\text{CAPE}}{dT}\right)$ and the contributions from changes in each of the parameters (each term on the right hand side of Equation 6) are expressed as relative rates of change (% K^{-1}) by scaling the rates of change (per degree K of SST warming) by the value of CAPE at 300 K. A residual is computed as the difference between the left and right hand sides of Equation 6. Unlike in Section 4, all calculations are done using parameter values specific to each model, so this decomposition assesses how changes in T_{LCL}, p_{LCL}, T_{LNB}, ϵ, PE_{theory}, and γ_{LCL} with warming in explain the change of CAPE with warming in each model.

Figure 9 shows the results of this decomposition. It is immediately evident that most of the CAPE increase with warming comes from warming of the atmosphere (T_{LCL}), which drives an increase in the saturation humidity at

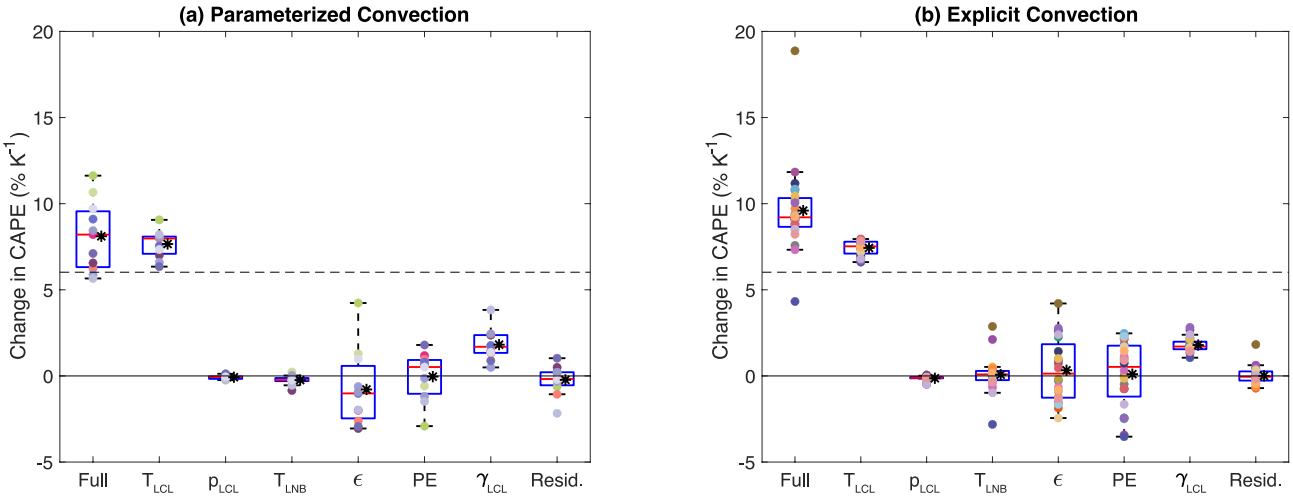

Figure 9. Changes in CAPE with warming and its decomposition into contributions from changes with warming of T_{LCL}, p_{LCL}, T_{LNB}, entrainment (ϵ), precipitation efficiency (PE), γ_{LCL}, and a residual (Resid.), from Equation 6, for (a) models with parameterized convection and (b) models with explicit convection. In the box plots, the red line is the median, the bottom and top edges of the box are the lower and upper quartiles, respectively, and the whiskers extend to 1.5 times the interquartile range. The black asterisk is the mean. The dashed black line is the change in CAPE with warming expected from Clausius-Clapeyron, based on the percent change in the saturation vapor pressure with warming, evaluated at 300 K.

cloud base. Changes in p_{LCL} have a negligible influence on CAPE and the residual is small. The contribution from changes in T_{LNB} is near zero in most models, generally consistent with small changes in anvil cloud temperatures (Stauffer & Wing, 2022). The average change in T_{LNB} is 0.1 K per degree of SST warming, which is a result of cancellation between the 21 models that exhibit a slight increase and the 17 that exhibit a slight decrease. Anvil cloud temperatures, on the other hand, increase slightly with warming across 84% of the `RCE_small` simulations at an average rate of 0.36 K per degree of SST warming (Stauffer & Wing, 2022), which is more consistent with the proportionally higher anvil temperature hypothesis (PHAT; Zelinka & Hartmann, 2010) than the fixed anvil temperature hypothesis (FAT; Hartmann & Larson, 2002). These differences notwithstanding, the results are consistent with the first order view that the temperature of the convecting top is relatively insensitive to warming. We note that there are two models (ICON-NWP-CRM and MicroHH) for which changes in T_{LNB} contribute more strongly to a ∼2%–3% K^{-1} increase in CAPE. These models exhibit the largest decreases in T_{LNB} (1.2–1.6 K cooling per degree SST warming), representing a deepening of the convecting layer. The model in which T_{LNB} has the largest negative contribution to CAPE changes, WRF-CRM, exhibits a 1.8 K warming of T_{LNB} per degree SST warming.

Increases in the water vapor scale height (γ^{-1}) across all models, or decreases in γ, contribute an additional increase in CAPE beyond that expected just from T_{LCL}, which helps increase CAPE beyond that expected from Clausius-Clapeyron. Indeed, Romps (2016) pointed out that under conditions where ϵ did not vary with warming, the temperature dependence of γ would further increase CAPE under warming. Across all models, γ_{LCL}^{-1} increases an average of 2.45% K^{-1}, while γ^{-1} averaged between 2 and 5 km increases an average of 4.30% K^{-1}. For reference, the average value of γ^{-1} between 2 and 5 km is 3.38 km and γ_{LCL}^{-1} is 2.94 km.

The contributions to CAPE changes from the remaining parameters, entrainment and precipitation efficiency (PE_{theory}), are scattered around zero and have the largest intermodel spread. This is consistent with Figure 8 and the conclusions from Section 4.3. The model-mean contributions of entrainment and PE_{theory} changes to CAPE changes are both near zero, particularly across CRMs. The models with parameterized convection are more likely to have decreases in entrainment with warming than those with explicit convection. Note that the entrainment contribution in Figure 9 reflects implied changes in entrainment at cloud base. The dependence of simulated γ on height implies an entrainment above cloud base that tends more toward a decrease with warming: 70% of the models exhibit a decrease in the 2–5 km average ϵ_z with warming while 30% exhibit an increase.

As noted earlier, ICON-NWP-CRM is an outlier, with a much larger increase in CAPE than other models (see also Figures 2 and 8). The decomposition in Figure 9 indicates this is due to a combination of contributions from an increase in entrainment, a decrease in T_{LNB}, and the residual, each of which is the largest of any model. Amongst the models with parameterized convection, the model with the largest increase in CAPE also has the largest entrainment contribution, largest T_{LCL} contribution, and smallest PE_{theory} contribution.

One somewhat unexpected result is that even the T_{LCL} contribution to changes in CAPE is greater than that expected from Clausius-Clapeyron. This is in apparent opposition to Romps (2016), who indicated that CAPE scaled with the surface saturation specific humidity over a wide range of temperatures (including those considered here). While changes in T_{LNB}, ϵ, PE_{theory}, or γ could modify this scaling, we find a super-Clausius-Clapeyron scaling even when those changes are excluded. The primary factor influencing this behavior is the fact that we compute changes with respect to 10 K of SST warming (305–295 K), but T_{LCL} increases at a slightly faster rate than SST. On average, T_{LCL} increases 10.9 K over the 10 K SST warming. Across models, T_{LCL} increases range from 9.45 to 12.99 K, and 34 out of the 38 models exhibit T_{LCL} increases that are greater than 10 K. Therefore, the saturation vapor pressure at cloud base increases more quickly than that at the SST (6.4% K^{-1} vs. 6.0% K^{-1}). If we compute the changes in CAPE and its decomposition with respect to changes in T_{LCL} rather than SST, the model-mean $\frac{\partial CAPE}{\partial T_{LCL}}$ is 6.9% K^{-1}, with a range of 6.6%–7.3% K^{-1}. This indicates that the ZBP model predicts an increase in CAPE based on changes in T_{LCL} that are very close to but slightly higher than that predicted by Clausius-Clapeyron. Another factor that may contribute is nonlinear behavior in CAPE (Equations A1–A4) that is neglected when we linearly decompose its contributions from each parameter (Equation 6). We also note that the value of the $\frac{dCAPE}{dT}$ contribution from T_{LCL} and how close it is to the Clausius-Clapeyron scaling is sensitive to whether we scale by the value of CAPE at 300 K or at 295 K (to compute a % K^{-1}) and which parameter values we use to compute the CAPE derivatives and the Clausius-Clapeyron scaling.

The above conclusions are broadly similar when we consider the subset of models with `RCE_small_vert` and `RCE_small_les` versions (Figure S6 in Supporting Information S1). In `RCE_small_les`, the entrainment contribution is more negative and the PE contribution is more positive than in its coarser resolution counterparts. The overall CAPE increase is slightly smaller in `RCE_small_les`, though still greater than that expected from Clausius-Clapeyron.

The above results are robust to the precise choice of heights used to average relative humidity when using the ZBP model to diagnose ϵ and PE_{theory}. The exact range of values for the entrainment and precipitation efficiency contributions vary somewhat for different height ranges (i.e., lean more toward negative or more toward positive), but are always spread on either side of zero. The intermodel spread in these contributions, and the residual, is smallest for ranges of heights close to 2–5 km, which is what we use.

6. Conclusions

While the RCE framework is simple in principle, there are many degrees of freedom in how the balance between convective heating and radiative cooling is obtained. Given the same domain size, resolution, boundary conditions, thermal forcing, and trace gas profiles, RCEMIP (Wing et al., 2018) made clear that there is no agreed upon RCE state, even if one excludes the complications of convective aggregation (Wing et al., 2020a). Furthermore, it is difficult to attribute the widely varying thermodynamic profiles (Figure 1) to any particular model characteristic, given the range of dynamical cores and subgrid scale parameterizations present in the RCEMIP ensemble.

Here, we leveraged recent theoretical developments to provide a physical understanding of what controls the intermodel spread in stability and relative humidity and its changes with warming in RCEMIP. We introduced a CAPE-RH phase space based on the ZBP model (Romps, 2014, 2016; Singh & O'Gorman, 2013) as a diagnostic tool to estimate values of entrainment and PE, and attribute variations in the simulated thermodynamic states to variations in these parameters. The theory-implied values of PE (PE_{theory}) agree well with microphysical PE (PE_{actual}) directly computed from a suite of perturbed physics simulations with a cloud-resolving model, lending confidence to our approach.

We found that models that are moister in the lower troposphere have greater instability (higher CAPE). This is qualitatively consistent with entrainment control of both properties, in which a higher entrainment rate results in greater CAPE, by leading to a larger lapse rate, and greater environmental humidity through an increase in convective detrainment. However, both theory-implied entrainment and PE_{theory} (as well as a proxy for PE, PE_{proxy}) vary across models. Using the ZBP model to perform a quantitative decomposition, we found that model-to-model variations in theory-implied entrainment explain most of the intermodel spread in CAPE and its changes with warming, but model-to-model variations in PE_{theory} explain the spread in relative humidity.

The lower-tropospheric relative humidity exhibits small changes with warming (the 5%–95% confidence interval is 0.03%–0.6% K^{-1}), consistent with theory and climate model simulations (Po-Chedley et al., 2019; Romps, 2014).

CAPE, on the other hand, increases strongly with warming, at a rate (average of 9.2% K^{-1}) larger than that expected from the Clausius-Clapeyron relation (6% K^{-1}). By deriving an analytical expression for the change in CAPE with warming based on the ZBP model, we decomposed the response of CAPE into contributions from changes in each of the six parameters (T_{LCL}, p_{LCL}, T_{LNB}, ϵ, PE, and γ_{LCL}). We confirmed that most of the CAPE increase with warming comes from the warming of the atmosphere itself, in which the increase in T_{LCL} drives an increase in saturation humidity at cloud base. Decreases in γ with warming, or increases in the water vapor scale height γ^{-1}, which are also ultimately linked to warming temperatures, contribute to additional increases in CAPE. The contribution from changes in the temperature of the convecting top T_{LNB} is near zero in most models.

The remaining parameters, entrainment and precipitation efficiency, do not exhibit a consistent change with warming and thus their contributions to CAPE changes are scattered around zero and have a large intermodel spread. Outlier changes in these parameters contribute to outlier changes in CAPE. The entrainment and precipitation efficiency contributions are more negative and more positive, respectively, in our limited subset of LES models. This indicates that entrainment changes might be sensitive to resolution, and it would be beneficial to confirm the theory-implied results here with more direct measures of entrainment.

On the other hand, our results do not support a substantial increase in PE with warming, as suggested by application of a proxy PE ($\mathrm{PE}_{\mathrm{proxy}}$) to RCEMIP and comprehensive GCM simulations (Li et al., 2022, 2023). Instead, we find that the theory-implied PE ($\mathrm{PE}_{\mathrm{theory}}$) change with warming, and thus its contribution to CAPE changes, is on average near-zero. However, this is slightly sensitive to the range of heights used to define lower-tropospheric relative humidity, and so the lack of agreement between $\mathrm{PE}_{\mathrm{theory}}$ and $\mathrm{PE}_{\mathrm{proxy}}$ with warming could reflect the height sensitivity of relative humidity changes, flaws in the ZBP theory, or limitations in the proxy, and we cannot rule out an increase in PE with warming. The large intermodel spread in both $\mathrm{PE}_{\mathrm{theory}}$ and $\mathrm{PE}_{\mathrm{proxy}}$ underlines our incomplete understanding of what sets PE and uncertainty in how it responds to warming.

Our conclusions are based on an analysis of the unaggregated `RCE_small` simulations. A natural extension of this work is thus to consider the influence of convective aggregation on the results found here. While it is known that the presence of aggregation substantially reduces mean relative humidity and enhances the dryness of dry regions (Wing, 2019; Wing et al., 2020a), this framework could be used to investigate how CAPE, entrainment, PE and their responses to warming are influenced by aggregation and *its* variability across models and with warming. Preliminary analysis suggests that the relationship between CAPE and relative humidity is qualitatively similar in the aggregated `RCE_large` simulations, but further investigation of the control of stability and relative humidity under conditions of convective aggregation is of great relevance to our understanding of climate feedbacks and changes in extremes (such as severe convective storms and heavy rainfall events) with warming.

Appendix A: CAPE and Its Derivatives

Romps (2016) used the ZBP model to derive an analytic equation for the CAPE given the temperature T_{LCL} and pressure p_{LCL} at the LCL, the temperature of the level of neutral buoyancy T_{LNB}, and the parameter $a = \epsilon PE\gamma_{\mathrm{LCL}}^{-1}$. This equation may be written

$$\mathrm{CAPE} = \frac{R_d}{2f}[\mathcal{G}(y_a, f, T_{\mathrm{LCL}}, T_{\mathrm{LNB}}) - \mathcal{G}(y_0, f, T_{\mathrm{LCL}}, T_{\mathrm{LNB}})], \tag{A1}$$

where the function $\mathcal{G}$ is defined below, R_d is the dry gas constant, and

$$f = \frac{L_v}{R_v T_0^2} - \frac{c_p}{R_d T_0}. \tag{A2}$$

Here L_v is the latent heat of vaporization, c_p is the isobaric specific heat capacity of dry air, and $T_0 = \frac{T_{\mathrm{LCL}} + T_{\mathrm{LNB}}}{2}$. The function $\mathcal{G}(y_a, f, T_{\mathrm{LCL}}, T_{\mathrm{LNB}})$ is given by

$$\begin{aligned}\mathcal{G}(y, f, T_{\mathrm{LCL}}, T_{\mathrm{LNB}}) = W(y)[2 - 2f(T_{\mathrm{LCL}} - T_{\mathrm{LNB}}) + W(y)] \\ -W\left(e^{-f(T_{\mathrm{LCL}} - T_{\mathrm{LNB}})}y\right)\left[2 + W\left(e^{-f(T_{\mathrm{LCL}} - T_{\mathrm{LNB}})}y\right)\right],\end{aligned} \tag{A3}$$

where $W(y)$ is the Lambert-W function (Romps, 2016), and y_a is given by

$$y_a = \frac{L_v q^*_{\mathrm{LCL}}}{(1+a)R_d T_0}\exp\left(\frac{L_v q^*_{\mathrm{LCL}}}{(1+a)R_d T_0}\right), \tag{A4}$$

where q^*_{LCL} is the saturation specific humidity at the LCL. The variable y_0 is given by y_a for $a = 0$.

To evaluate the sensitivity of the CAPE described by Equations A1–A4 to its input parameters, we calculate the partial derivatives of the CAPE with respect to the six input arguments represented by the vector $\mathbf{x} = (T_{\mathrm{LCL}}, p_{\mathrm{LCL}}, T_{\mathrm{LNB}}, \epsilon, \mathrm{PE}, \gamma_{\mathrm{LCL}})$. By the chain rule we have that,

$$\frac{\partial \mathrm{CAPE}}{\partial \mathbf{x}} = -\frac{\mathrm{CAPE}}{f}\frac{\partial f}{\partial \mathbf{x}} + \frac{R_d}{2f}\left[\frac{\partial \mathcal{G}}{\partial y}\frac{\partial y}{\partial \mathbf{x}} + \frac{\partial \mathcal{G}}{\partial f}\frac{\partial f}{\partial \mathbf{x}} + \frac{\partial \mathcal{G}}{\partial T_{\mathrm{LCL}}}\frac{\partial T_{\mathrm{LCL}}}{\partial \mathbf{x}} + \frac{\partial \mathcal{G}}{\partial T_{\mathrm{LNB}}}\frac{\partial T_{\mathrm{LNB}}}{\partial \mathbf{x}}\right]_0^a, \tag{A5}$$

where the term in square brackets is given by the difference in its value at the given value of a, and at $a = 0$. Evaluating the partial derivatives of $\mathcal{G}$ we have,

$$\begin{aligned}\frac{\partial \mathcal{G}}{\partial y} &= [2 - 2f(T_{\mathrm{LCL}} - T_{\mathrm{LNB}}) + 2W(y)]W_y(y),\\ &\quad - \left[2 + 2W\left(e^{-f(T_{\mathrm{LCL}}-T_{\mathrm{LNB}})}y\right)\right]W_y\left(e^{-f(T_{\mathrm{LCL}}-T_{\mathrm{LNB}})}y\right)e^{-f(T_{\mathrm{LCL}}-T_{\mathrm{LNB}})},\end{aligned} \tag{A6}$$

$$\frac{\partial \mathcal{G}}{\partial f} = -2(T_{\mathrm{LCL}} - T_{\mathrm{LNB}})W(y) + (2 + 2W(y))W_y(y)e^{-f(T_{\mathrm{LCL}}-T_{\mathrm{LNB}})}y(T_{\mathrm{LCL}} - T_{\mathrm{LNB}}), \tag{A7}$$

$$\frac{\partial \mathcal{G}}{\partial T_{\mathrm{LCL}}} = -2fW(y) + f(2 + 2W(y))W_y(y)ye^{-f(T_{\mathrm{LCL}}-T_{\mathrm{LNB}})}, \tag{A8}$$

$$\frac{\partial \mathcal{G}}{\partial T_{\mathrm{LNB}}} = 2fW(y) - f(2 + 2W(y))W_y(y)ye^{-f(T_{\mathrm{LCL}}-T_{\mathrm{LNB}})}. \tag{A9}$$

Here

$$W_y(y) = \frac{\partial W}{\partial y} = \frac{W(y)}{y(1 + W(y))} \tag{A10}$$

is the derivative of the Lambert-W function with respect to its argument. We now evaluate the partial derivatives with respect to the input vector $\mathbf{x}$. For T_{LCL} and T_{LNB} this is trivial,

$$\frac{\partial T_{\mathrm{LCL}}}{\partial \mathbf{x}} = (1, 0, 0, 0, 0), \tag{A11}$$

$$\frac{\partial T_{\mathrm{LNB}}}{\partial \mathbf{x}} = (0, 0, 1, 0, 0). \tag{A12}$$

For f and y, we have

$$\frac{\partial f}{\partial \mathbf{x}} = \left[-\frac{2L_v}{R_v T_0} + \frac{c_p}{R_d T_0^3}\right]\left(\frac{1}{2}, 0, \frac{1}{2}, 0, 0\right) \tag{A13}$$

$$\frac{\partial y}{\partial \mathbf{x}} = \left[\exp(z) + z\exp(z)\right]\frac{\partial z}{\partial \mathbf{x}} \tag{A14}$$

where we have defined

$$z = \frac{L_v q^*_{\mathrm{LCL}}}{(1+a)R_d T_0}. \tag{A15}$$

Using the definition of the saturation specific humidity and the Clausius-Clapeyron equation, we may write the derivatives of q^*_{LCL} as:

$$\frac{\partial q^*_{\mathrm{LCL}}}{\partial T_{\mathrm{LCL}}} = \left(1 + \left(\frac{R_v}{R_d} - 1\right)q^*_{\mathrm{LCL}}\right)\frac{L_v q^*_{\mathrm{LCL}}}{R_v T^2_{\mathrm{LCL}}}, \tag{A16}$$

$$\frac{\partial q^*_{\mathrm{LCL}}}{\partial p_{\mathrm{LCL}}} = -\left(1 + \left(\frac{R_v}{R_d} - 1\right) q^*_{\mathrm{LCL}}\right) \frac{q^*_{\mathrm{LCL}}}{p_{\mathrm{LCL}}}. \tag{A17}$$

This allows us to write the partial derivatives of z as,

$$\frac{\partial z}{\partial T_{\mathrm{LCL}}} = \left(1 + \left(\frac{R_v}{R_d} - 1\right) q^*_{\mathrm{LCL}}\right) \frac{L_v^2 q^*_{\mathrm{LCL}}}{(1+a) R_d R_v T_0 T_{\mathrm{LCL}}^2} - \frac{L_v q^*_{\mathrm{LCL}}}{2(1+a) R_d T_0^2}, \tag{A18}$$

$$\frac{\partial z}{\partial p_{\mathrm{LCL}}} = \left(1 + \left(\frac{R_v}{R_d} - 1\right) q^*_{\mathrm{LCL}}\right) \frac{L_v q^*_{\mathrm{LCL}}}{p_{\mathrm{LCL}}(1+a) R_d T_0}, \tag{A19}$$

$$\frac{\partial z}{\partial T_{\mathrm{LNB}}} = -\frac{L_v q^*_{\mathrm{LCL}}}{2(1+a) R_d T_0^2}, \tag{A20}$$

$$\frac{\partial z}{\partial a} = -\frac{L_v q^*_{\mathrm{LCL}}}{(1+a)^2 R_d T_0}. \tag{A21}$$

Finally, the derivatives of a may be written,

$$\frac{\partial a}{\partial \epsilon} = \mathrm{PE}/\gamma_{\mathrm{LCL}}, \tag{A22}$$

$$\frac{\partial a}{\partial \mathrm{PE}} = \epsilon/\gamma_{\mathrm{LCL}}, \tag{A23}$$

$$\frac{\partial a}{\partial \gamma_{\mathrm{LCL}}} = -\epsilon \mathrm{PE}/\gamma^2_{\mathrm{LCL}}. \tag{A24}$$

These previous three equations combined with A21 allow for evaluations of the derivative of z with respect to ϵ, PE and γ_{LCL}. Using Equations A6–A24 we may therefore evaluate the partial derivatives of CAPE with respect to each element of $\mathbf{x}$, providing the terms required in Equation 6.

Data Availability Statement

The standardized RCEMIP data (Wing et al., 2020b) is hosted by the German Climate Computing Center (DKRZ) and is publicly available online at http://hdl.handle.net/21.14101/d4beee8e-6996-453e-bbd1-ff53b6874c0e. The RCEMIP data set includes the original model data as well as post-processed statistics, including the time- and domain-mean profiles used here. Other data derived from RCEMIP for this study, data from the perturbed physics simulations, and the analysis scripts are in a Zenodo repository at https://doi.org/10.5281/zenodo.10140830 (Wing & Singh, 2023).

Acknowledgments
We thank all co-authors on the RCEMIP overview paper (Wing et al., 2020a) for providing the RCEMIP simulations and we thank the German Climate Computing Center (DKRZ) for hosting the standardized RCEMIP data. We also thank Catherine Stauffer and Graham O'Donnell for their assistance in processing the RCEMIP data. We also thank Tristan Abbott and an anonymous reviewer for thoughtful and constructive feedback on the paper. A. A. Wing acknowledges support from the NSF Grants AGS 1830724 and AGS 2140419. M. S. Singh acknowledges support from the Australian Research Council through Grants DE190100866 and CE170100023, support from the Max Planck Society, and resources and services from the National Computational Infrastructure (NCI), which is supported by the Australian Government.

References

Becker, T., & Wing, A. A. (2020). Understanding the extreme spread in climate sensitivity within the Radiative-Convective Equilibrium Model Intercomparison Project. *Journal of Advances in Modeling Earth Systems*, *12*(10), e2020MS002165. https://doi.org/10.1029/2020ms002165

Braun, S. A., & Tao, W.-K. (2000). Sensitivity of high-resolution simulations of Hurricane Bob (1991) to planetary boundary layer parameterizations. *Monthly Weather Review*, *128*(12), 3941–3961. https://doi.org/10.1175/1520-0493(2000)129<3941:sohrso>2.0.co;2

Brooks, H. E., III., Doswell, C. A., & Cooper, J. (1994). On the environments of tornadic and nontornadic mesoscyclones. *Weather and Forecasting*, *9*(4), 606–618. https://doi.org/10.1175/1520-0434(1994)009<0606:oteota>2.0.co;2

Bryan, G. H., & Fritsch, J. M. (2002). A benchmark simulation for moist nonhydrostatic numerical models. *Monthly Weather Review*, *130*(12), 2917–2928. https://doi.org/10.1175/1520-0493(2002)130⟨2917:ABSFMN⟩2.0.CO;2

Colman, R., & Soden, B. J. (2021). Water vapor and lapse rate feedbacks in the climate system. *Reviews of Modern Physics*, *93*(4), 045002. https://doi.org/10.1103/RevModPhys.93.045002

Diao, M., Bryan, G. H., Morrison, H., & Jensen, J. B. (2017). Ice nucleation parameterization and relative humidity distribution in idealized squall-line simulations. *Journal of the Atmospheric Sciences*, *74*(9), 2761–2787. https://doi.org/10.1175/JAS-D-16-0356.1

Diffenbaugh, N. S., Scherer, M., & Trapp, R. J. (2013). Robust increases in severe thunderstorm environments in response to greenhouse forcing. *Proceedings of the National Academy of Sciences of the United States of America*, *110*(41), 16361–16366. https://doi.org/10.1073/pnas.1307758110

Douglass, D. H., Christy, J. R., Pearson, B. D., & Singer, S. F. (2008). A comparison of tropical temperature trends with model predictions. *International Journal of Climatology*, *28*(13), 1693–1701. https://doi.org/10.1002/joc.1651

Hartmann, D. L., & Larson, K. (2002). An important constraint on tropical cloud-climate feedback. *Geophysical Research Letters*, *29*(20), 12-1–12-4. https://doi.org/10.1029/2002GL015835

Lepore, C., Abernathey, R., Henderson, N., Allen, J. T., & Tippett, M. K. (2021). Future global convective environments in CMIP6 models. *Earth's Future*, *9*(12). https://doi.org/10.1029/2021EF002277

Li, R. L., Studholme, J. H. P., Fedorov, A. V., & Storelvmo, T. (2022). Precipitation efficiency constraint on climate change. *Nature Climate Change*, *12*(7), 642–648. https://doi.org/10.1038/s41558-022-01400-x

Li, R. L., Studholme, J. H. P., Fedorov, A. V., & Storelvmo, T. (2023). Increasing precipitation efficiency amplifies climate sensitivity by enhancing tropical circulation slowdown and eastern Pacific warming pattern. *Geophysical Research Letters*, *50*(2), e2022GL100836. https://doi.org/10.1029/2022GL100836

Lin, Y.-L., Farley, R. D., & Orville, H. D. (1983). Bulk parameterization of the snow field in a cloud model. *Journal of Climate and Applied Meteorology*, *22*(6), 1065–1092. https://doi.org/10.1175/1520-0450(1983)022<1065:bpotsf>2.0.co;2

Manabe, S., & Stouffer, R. J. (1980). Sensitivity of a global climate model to an increase in CO_2 concentration in the atmosphere. *Journal of Geophysical Research*, *85*(C10), 5529–5554. https://doi.org/10.1029/jc085ic10p05529

Manabe, S., & Strickler, R. F. (1964). Thermal equilibriation of the atmosphere with a convective adjustment. *Journal of the Atmospheric Sciences*, *21*(4), 361–385. https://doi.org/10.1175/1520-0469(1964)021<0361:teotaw>2.0.co;2

Manabe, S., & Wetherald, R. T. (1967). Thermal equilibrium of the atmosphere with a given distribution of relative humidity. *Journal of the Atmospheric Sciences*, *24*(3), 241–259. https://doi.org/10.1175/1520-0469(1967)024<0241:teotaw>2.0.co;2

Pendergrass, A. G. (2020). Changing degree of convective organization as a mechanisms for dynamic changes in extreme precipitation. *Current Climate Change Reports*, *6*(2), 47–54. https://doi.org/10.1007/s40641-020-00157-9

Po-Chedley, S., Zelinka, M. D., Jeevanjee, N., Thorsen, T. J., & Santer, B. D. (2019). Climatology explains intermodel spread in tropical upper tropospheric cloud and relative humidity response to greenhouse warming. *Geophysical Research Letters*, *46*(22), 13399–13409. https://doi.org/10.1029/2019GL084786

Romps, D. M. (2010). A direct measure of entrainment. *Journal of the Atmospheric Sciences*, *67*(6), 1908–1927. https://doi.org/10.1175/2010JAS3371.1

Romps, D. M. (2014). An analytical model for tropical relative humidity. *Journal of Climate*, *27*(19), 7432–7449. https://doi.org/10.1175/JCLI-D-14-00255.1

Romps, D. M. (2016). Clausius-Clapeyron scaling of CAPE from analytical solutions to RCE. *Journal of the Atmospheric Sciences*, *73*(9), 3719–3737. https://doi.org/10.1175/jas-d-15-0327.1

Romps, D. M. (2017). Exact expression for the lifting condensation level. *Journal of the Atmospheric Sciences*, *74*(12), 3891–3900. https://doi.org/10.1175/JAS-D-17-0102.1

Romps, D. M. (2021). The Rankine-Kirchoff approximations for moist thermodynamics. *The Quarterly Journal of the Royal Meteorological Society*, *147*(740), 3493–3497. https://doi.org/10.1002/qj.4154

Romps, D. M., Seeley, J. T., Vollaro, D., & Molinari, J. (2014). Projected increase in lightning strikes in the United States due to global warming. *Science*, *346*(6211), 851–854. https://doi.org/10.1126/science.1259100

Santer, B. D., Solomon, S., Pallotta, G., Mears, C., Po-Chedley, S., Fu, Q., et al. (2017). Comparing tropospheric warming in climate models and satellite data. *Journal of Climate*, *30*(1), 373–392. https://doi.org/10.1175/JCLI-D-16-0333.1

Santer, B. D., Thorne, P. W., Haimberger, L., Taylor, K. E., Wigley, T. M. L., Lanzante, J. R., et al. (2008). Consistency of modelled and observed temperature trends in the tropical troposphere. *International Journal of Climatology*, *28*(13), 1703–1722. https://doi.org/10.1002/joc.1756

Seeley, J. T., & Romps, D. M. (2015). Why does tropical convective available potential energy (CAPE) increase with warming? *Geophysical Research Letters*, *42*(23), 10429–10437. https://doi.org/10.1002/2015GL066199

Singh, M. S., Kuang, Z., Maloney, E. D., Hannah, W. M., & Wolding, B. O. (2017). Increasing potential for intense tropical and subtropical thunderstorms under global warming. *Proceedings of the National Academy of Sciences of the United States of America*, *114*(44), 11657–11662. https://doi.org/10.1073/pnas.1707603114

Singh, M. S., & O'Gorman, P. (2013). Influence of entrainment on the thermal stratification in simulations of radiative-convective equilibrium. *Geophysical Research Letters*, *40*(16), 4398–4403. https://doi.org/10.1002/glr.50796

Singh, M. S., Warren, R. A., & Jakob, C. J. (2019). A steady-state model for the relationship between humidity, instability, and precipitation in the tropics. *Journal of Advances in Modeling Earth Systems*, *11*(12), 3973–3994. https://doi.org/10.1029/2019MS001686

Stauffer, C. L., & Wing, A. A. (2022). Properties, changes, and controls of deep-convecting clouds in radiative-convective equilibrium. *Journal of Advances in Modeling Earth Systems*, *14*(6), e2021MS002917. https://doi.org/10.1029/2021MS002917

Tao, W.-K., & Simpson, J. (1993). The Goddard cumulus ensemble model. Part I: Model description. *Terrestrial, Atmospheric and Oceanic Sciences*, *4*, 35–72.

Wagner, W., & Pruß, A. (2002). The IAPWS formulation 1995 for the thermodynamic properties of ordinary water substance for general and scientific use. *Journal of Physical and Chemical Reference Data*, *31*(2), 387–535. https://doi.org/10.1063/1.1461829

Wagner, W., Riethmann, T., Feistel, R., & Harvey, A. H. (2011). New equations for the sublimation pressure and melting pressure of H_2O ice Ih. *Journal of Physical and Chemical Reference Data*, *40*(4), 043103. https://doi.org/10.1063/1.3657937

Wing, A. A. (2019). Self-aggregation of deep convection and its implications for climate. *Current Climate Change Reports*, *5*, 1–11. https://doi.org/10.1007/s40641-019-00120-3

Wing, A. A., Emanuel, K., Holloway, C. E., & Muller, C. (2017). Convective self-aggregation in numerical simulations: A review. *Surveys in Geophysics*, *38*(6), 1173–1197. https://doi.org/10.1007/s10712-017-9408-4

Wing, A. A., Reed, K. A., Satoh, M., Stevens, B., Bony, S., & Ohno, T. (2018). Radiative-convective equilibrium model intercomparison project. *Geoscientific Model Development*, *11*(2), 793–813. https://doi.org/10.5194/gmd-11-793-2018

Wing, A. A., & Singh, M. S. (2023). allison-wing/RH_stability: v1.0 (v1.0) [Dataset, Software]. Zenodo. https://doi.org/10.5281/zenodo.10140830

Wing, A. A., Stauffer, C., Becker, T., Reed, K., Ahn, M.-S., Arnold, N., et al. (2020a). Clouds and convective self-aggregation in a multi-model ensemble of radiative-convective equilibrium simulations. *Journal of Advances in Modeling Earth Systems*, *12*(9), e2020MS002138. https://doi.org/10.1029/2020MS002138

Wing, A. A., Stauffer, C., Becker, T., Reed, K., Ahn, M.-S., Arnold, N., et al. (2020b). Radiative-convective equilibrium model intercomparison project (RCEMIP) simulation dataset [Dataset]. WDC Climate. Retrieved from http://hdl.handle.net/21.14101/d4beee8e-6996-453e-bbd1-ff53b6874c0e

Zelinka, M., & Hartmann, D. (2010). Why is longwave cloud feedback positive? *Journal of Geophysical Research*, *115*(D16), D16117. https://doi.org/10.1029/2010JD013817